Reactor transfer function measurements with

the reactor oscillator

by

Te-Chang Chan

A Thesis Submitted to the

Graduate Faculty in Partial Fulfillment of

The Requirements for the Degree of

MASTER OF SCIENCE

Major Subject: Nuclear Engineering

Iowa State University
Ames, Iowa

1971

TABLE OF CONTENTS

I. INTRODUCTION

The ultimate purpose of the construction and operation of a nuclear reactor is to provide a useful source of energy in the form of heat and/or nuclear radiation. In order to be useful, a nuclear reactor must be controllable under a set of known conditions and circumstances. One of the most important aspects of a reactor's controllability, that must be known to insure safe operation, is the reactor's dynamic response to changes in operating conditions. Consequently, the analysis of the dynamic behavior of reactors and reactor power plants is of the utmost importance in both the design and the operation stages of the plant.

The most frequently employed method of analyzing the dynamic response of a system is to observe the system's response in terms of the gain and phase angle between input and output for a sinusoidally varying input. This response information is then utilized to plot the transfer characteristic or transfer function of the system. The observed transfer function may then be analyzed to yield information about the stability of the system and to establish parameters for the system in theoretical studies.

This transfer function measuring technique is closely related to the reactor-oscillator method used in this thesis. The transfer function of interest is the open loop and the closed loop transfer function of the UTR-10 reactor.

A. Open Loop Transfer
Function

The transfer function of a system is defined as the ratio
of the Laplace transform of the output to the input with zero
initial conditions on the output. In the present case the
output is normally considered to be a small amplitude variation
in the neutron level and the input is a small sinusoidal
varying reactivity. That is

$$G(s) = \frac{\mathcal{L}(\text{output neutron variation})}{\mathcal{L}(\text{input reactivity variation})} = \frac{\Delta N(s)}{\Delta K(s)} \qquad (1)$$

where $G(s)$ is the transfer function, $\Delta N(s)/\Delta K(s)$ is the La-
place transform of the function that describes all of the
input reactivity variations. The term, transfer function, is
derived from the fact that the transform of the output
response of a system is equal to the transform of the input
multiplied by the transfer function of the system.

The open loop or zero power transfer function of a nuclear
reactor is the transfer function of the reactor based only on
delayed neutron effects and neglecting all feedback effects.
This type of transfer function is easily measured by means
of pile oscillation techniques and may be theoretically formu-
lated quite simply from the space independent reactor kinetic
equations. The open loop transfer function given by Schultz
[24] is

$$G(s) = \frac{\Delta N(s)}{\Delta K(s)} = \frac{n(0)}{\ell s[1 + \sum\limits_{i=1}^{6} \frac{\beta_i}{\ell(s+\lambda_i)}]} \quad . \tag{2}$$

In block diagram notation, Equation (2) can be used to represent the reactor as shown in Figure 1.

B. Closed Loop Transfer Function

The closed loop or power transfer function of a nuclear is the complete transfer function including all feedback effects. A simple closed loop transfer function of a reactor with one feedback loop is depicted in Figure 2.

Mathematically, the transfer function of the loop in Figure 2 is given by

$$R(s) = \frac{\Delta N(s)}{\Delta K(s)} = \frac{K_1 G(s)}{1 + K_1 K_2 G(s) H(s)} \tag{3}$$

where K_1 is the frequency independent portion of the reactor transfer function $K_1 G(s)$ and K_2 is the frequency independent portion of the feedback function $K_2 H(s)$.

The closed loop transfer function of a reactor describes the dynamic behavior of the system with its associated equipment and, consequently, is of more practical importance to reactor design and operation than a simple open loop transfer function. However, the closed loop transfer function of a large reactor and its associated equipment is complex and more

$$\Delta K(S) \longrightarrow \boxed{\dfrac{n(0)}{\ell S\left[1 + \displaystyle\sum_{i=1}^{6} \dfrac{\beta_i}{\ell(S+\lambda_i)}\right]}} \longrightarrow \Delta N(S)$$
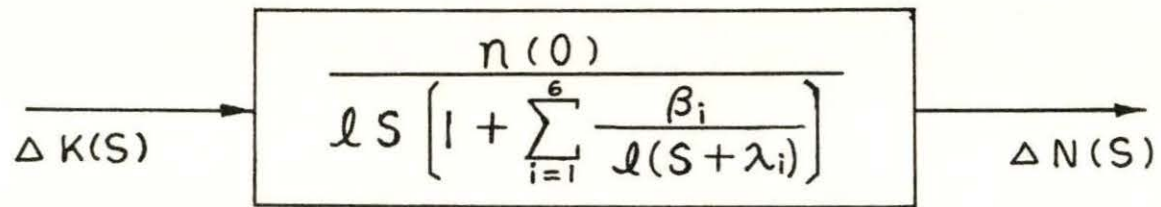
FIGURE 1. BLOCK DIAGRAM OF THE OPEN LOOP REACTOR TRANSFER
FUNCTION
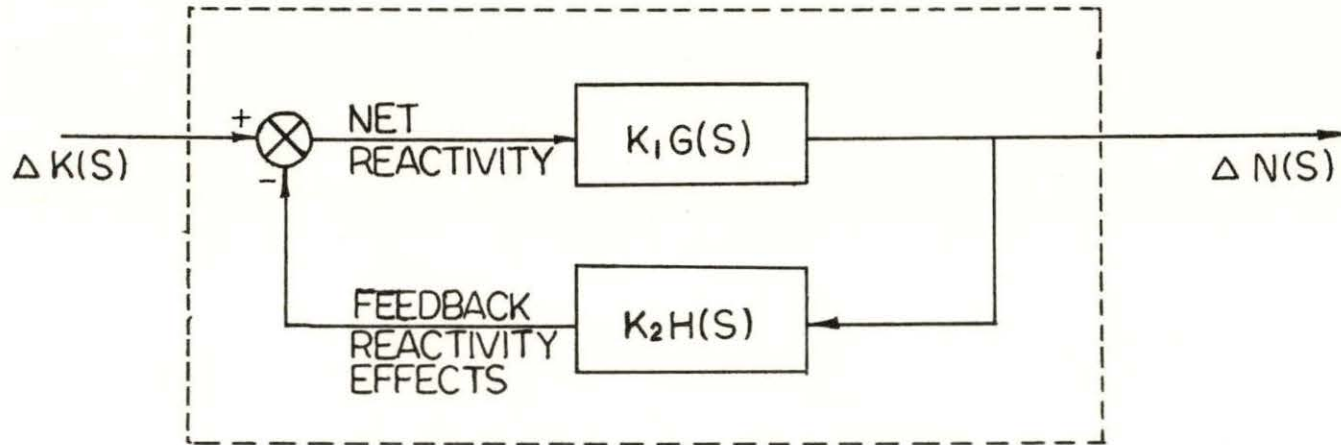
FIGURE 2. BLOCK DIAGRAM OF THE FEEDBACK LOOP TRANSFER FUNCTION

Amperes

$$1.5 \times 10^{-8}$$

ION CHAMBER

ΔP

$$\frac{P(0)}{\ell S \left[1 + \sum_{i=1}^{6} \frac{\beta_i}{\ell (S + \lambda_i)} \right]}$$

REACTOR

ΔK

ΔP

ΔK

Reactivity

$$1.15 \times 10^{-4}$$

$$\left(\frac{10^6}{\frac{S}{4} + 1} \right) \left(\frac{10^{-6}}{\text{Setting}} \right)$$ MICROMICROAMMETER

$$\frac{1.35 \times 10^{-15} Q}{\left(\frac{S}{0.0136} + 1 \right) \left(\frac{S}{0.069} + 1 \right)}$$

TEMPERATURE COEFFICIENT

Rod position

$$16.8$$

Volts

$$\frac{10}{\frac{S}{25} + 1}$$ RECORDER

CONTROLLER

$$\frac{0.167 \, I \left(\frac{S^2}{1/60T} + \frac{S}{1/60T} + 1 \right)}{\alpha \, P\% \, S}$$

$-$ Error

Recorder slidewire position

$+$

Set point slidewire position

Rod slidewire position
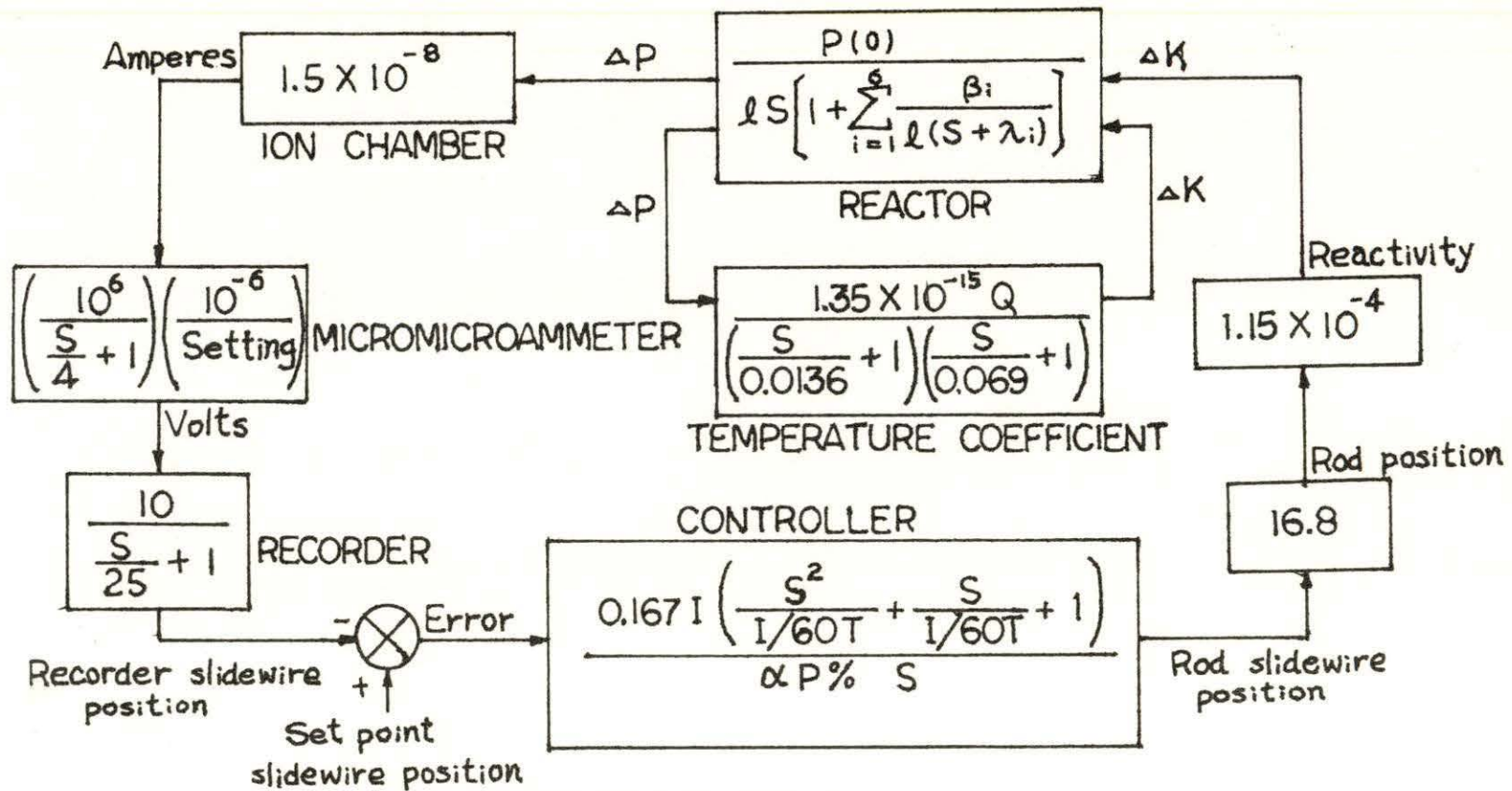
LEGEND :
P%   IS PROPORTIONAL BAND ADJ.
I   IS RESET RESPONSE ADJ.
T   IS RATE RESPONSE ADJ.
α IS FRACTION OF FULL SCALE SETTING

FIGURE 3. BLOCK DIAGRAM FURNISHED BY REACTOR MANUFACTURER

9

difficult to formulate theoretically due to the presence of numerous feedback loops. The number and arrangement of these loops is dependent upon the particular type of reactor, the amount and arrangement of the reactors associated equipment, and the analytical model chosen to represent the system.

The block diagram of the UTR-10 reactor and control system supplied by the manufacturer's representative [23] is given in Figure 3. When the reactor is operated at a low power level, the temperature feedback is small and may be neglected. From Figure 3, the feedback transfer function is obtained as

$$H(s) = K_2 \frac{s^2 + \frac{1}{T} s + \frac{1}{60T}}{s(s+4)(s+25)} . \tag{4}$$

At sufficiently high frequencies, the feedback transfer function H(s) approaches zero. Thus the open loop and the closed loop transfer function are the same at high frequencies.

C. Cross-correlation Technique

The measurement of the frequency response of a reactor requires the observation of a small signal in the presence of noise and the steady state component of the neutron flux signal. The techniques of cross-correlation are used to obtain accurate information about system response in the presence of extraneous noise signals in a minimum time. The basic mathematical

description of this technique is given by Harrer [15] and will be presented here.

Two functions $f(t)$ and $g(t)$ can be cross-correlated to obtain the function

$$\Psi_{fg}(\tau) = \lim_{T\to\infty} \frac{1}{2T} \int_{-T}^{T} f(t)g(t+\tau)\,dt \quad . \tag{5}$$

For a reactor, $f(t)$ can be written

$$f(t) = N(t) + n_0 + n_1 \sin(\omega t + \phi) \tag{6}$$

where $N(t)$ represents the noise signal, n_0 the steady state signal and $n_1 \sin(\omega t + \phi)$ the frequency response of the reactor. The function $g(t)$ is the input to the reactor, which in the case of frequency response measurements is

$$g(t) = A \sin\omega t \quad . \tag{7}$$

In this case, Equation (5) becomes

$$\Psi_{fg}(\tau) = \lim_{T\to\infty} \frac{1}{2T} \int_{-T}^{T} [N(t) + n_0 + n_1 \sin(\omega t + \phi)]$$

$$[A \sin\omega(t+\tau)]\,dt.$$

For $\tau = 0$

$$\Psi_{fg}(0) = \lim_{T\to\infty} \frac{1}{2T} \int_{-T}^{T} [N(t) + n_0 + n_1 \sin(\omega t + \phi)]$$

$$[A \sin\omega t]\,dt \quad . \tag{8}$$

Experimental data are taken for a finite interval and if an integral number of cycles are observed the total positive time T is

$$T = \frac{K}{f}$$

where K is an integer 1, 2, 3 etc., and f is the frequency in Hz. Changing the lower limit of Equation (8) to 0 and replacing the infinite limit by the finite time T, Equation (8) becomes

$$\Psi_{fg}(0) = \frac{fA}{K} \int_0^{K/f} N(t) \sin\omega t \, dt + \frac{fA}{K} \int_0^{K/f} n_0 \sin\omega t \, dt$$

$$+ \frac{fA}{K} \int_0^{K/f} n_1 \sin(\omega t+\phi) \sin\omega t \, dt \,. \qquad (9)$$

The mean value of N(t) is zero and there is no correlation between N(t) and A $\sin\omega t$, thus the first term is zero when K is integer. The second term is zero since n_0 is constant and the integral of $\sin\omega t$ is zero for integer K. The resulting expression for $\Psi_{fg}(0)$ is

$$\Psi_{fg}(0) = \frac{fA}{K} \int_0^{K/f} n_1 \sin(\omega t+\phi) \sin\omega t \, dt \qquad (10)$$

and using the formula

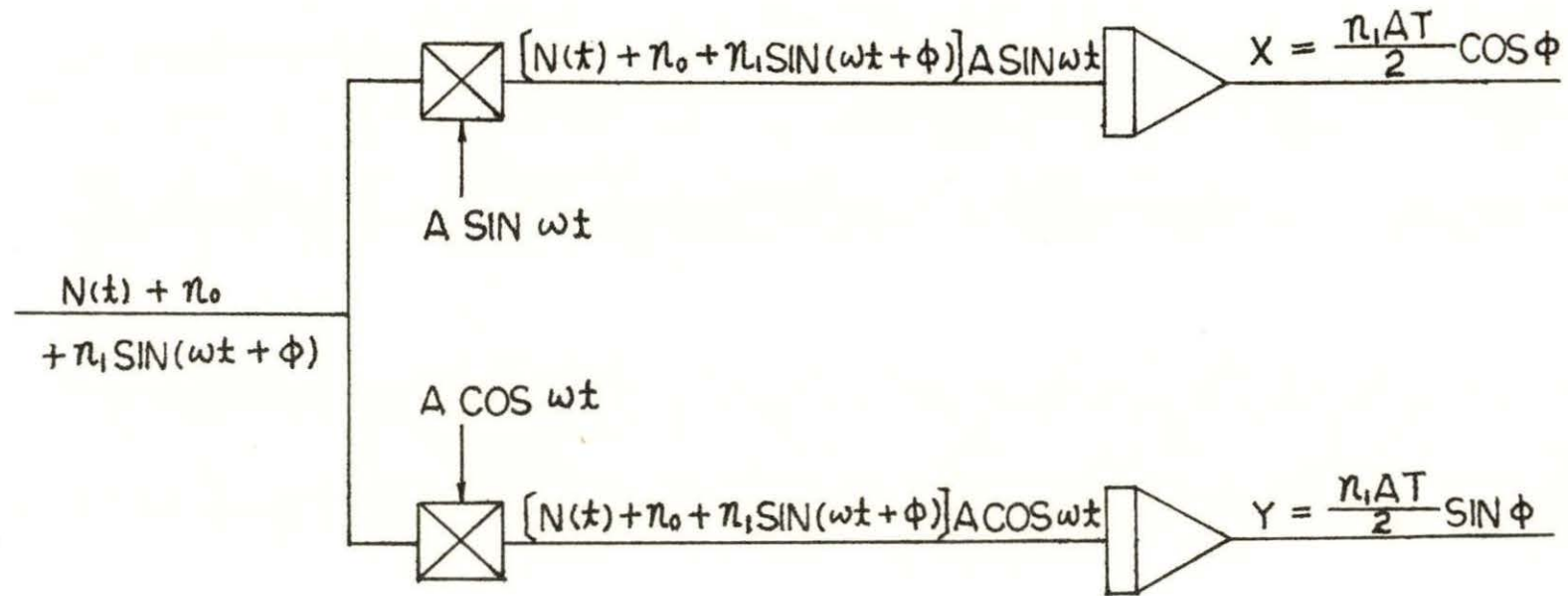$$\sin(\omega t+\phi) = \sin\omega t \cos\phi + \cos\omega t \sin\phi$$

Equation (10) becomes

FIGURE 4. CROSS-CORRELATION METHOD FOR FREQUENCY RESPONSE
MEASUREMENT

$$\Psi_{fg}(0) = \frac{fAn_1}{K} \cos\phi \int_0^{K/f} \sin^2\omega t \, dt$$

$$+ \frac{fAn_1}{K} \sin\phi \int_0^{K/f} \sin\omega t \, \cos\omega t \, dt \, .$$

The second integral is zero and the first integral can be written as

$$\Psi_{fg}(0) = \frac{fAn_1}{K} \cos\phi \int_0^{K/f} (\frac{1}{2} - \frac{1}{2} \cos 2\omega t) \, dt$$

$$= \frac{An_1}{2} \cos\phi \, . \tag{11}$$

When in particular $\tau = 1/4f$, then $\sin\omega(t+\tau)$ becomes $\cos\omega t$ and the result is

$$\Psi_{fg}(1/4f) = \frac{fA}{K} \int_0^{K/f} n_1 \sin(\omega t+\phi) \cos\omega t \, dt$$

$$= \frac{An_1}{2} \sin\phi. \tag{12}$$

Figure 4 shows the method for carrying out the cross-correaltion. The functions $A \sin\omega t$ and $A \cos\omega t$ are obtained from a sin-cos potentiometer which is coupled to the oscillator.

The output X and Y can be used to obtain the amplitude and phase angle

$$n_1 = \frac{2}{AT} \sqrt{X^2+Y^2} \tag{13}$$

$$\phi = \tan^{-1} (\frac{Y}{X}) \tag{14}$$

where T is the integration time. n_1 can be obtained to any degree of accuracy desired, if the number of cycles can be made exactly an integer.

At low frequency the use of an exact number of cycles is important but not difficult to control. At high frequencies more difficulty is experienced in terminating the measurement at the end of a cycle, but a large number of cycles can be run in a short time, and keeping the number exactly an integer is not as important.

D. Reactor Transfer Function
Measurement

In applying the cross-correlation technique to transfer function measurement, the input signal corresponding to Equation (7) is obtained from the reactivity oscillator. An error θ in the angular setting of the coupling of the sin-cos potentiometer and oscillator results in a corresponding phase error of the sin-cos functions in relation to the actual reactivity oscillations. It will be seen later that this error θ is eliminated by running the oscillator in both the forward and reverse directions and then using the average of the two results as the correct value of the phase shift. The output signal $f(t)$ can now be represented by

$$f_1(t) = N(t) + n_0 + n_1 \sin(\omega t + \phi) \tag{15}$$

in the forward direction and

$$f_2(t) = N(t) + n_0 - n_1 \sin(\omega t + \phi) \tag{16}$$

in the reverse direction.

The sin-cos functions generated are represented by

$$g_1(t) = A \sin(\omega t + \theta) \tag{17}$$

$$g_1'(t) = A \cos(\omega t + \theta) \tag{18}$$

in the forward direction and

$$g_2(t) = -A \sin(\omega t - \theta) \tag{19}$$

$$g_2'(t) = A \cos(\omega t - \theta) \tag{20}$$

in the reverse direction.

For the forward rotation of the oscillator, multiplication of the signals $f_1(t)$ and $g_1(t)$ and integration of the product for time T_1 gives

$$X_1 = \int_0^{T_1} [N(t) + n_0 + n_1 \sin(\omega t + \phi)][A \sin(\omega t + \theta)]dt$$

$$= \frac{An_1 T_1}{2} \cos(\phi - \theta) . \tag{21}$$

Multiplication of signals $f_1(t)$ and $g_1'(t)$ and integration of the product for time T_1 gives

$$Y_1 = \int_0^{T_1} [N(t) + n_0 + n_1 \sin(\omega t + \phi)][A \cos(\omega t + \theta)]dt$$

$$= \frac{An_1 T_1}{2} \sin(\phi - \theta). \tag{22}$$

For the reverse rotation of the oscillator, multiplication of signals $f_2(t)$ and $g_2(t)$ and integration of the product for

time T_2 gives

$$X_2 = \frac{An_1T_2}{2} \cos(\phi+\theta) \tag{23}$$

and similarly the multiplication of signals $f_2(t)$ and $g_2'(t)$ and integration of the product gives

$$Y_2 = -\frac{An_1T_2}{2} \sin(\phi+\theta) . \tag{24}$$

Equations (21) through (24) yield the amplitude n_1 and phase angle ϕ in the forward and reverse directions as shown in Equations (25) through (28).

With forward rotation:

$$n_1 = \frac{2}{AT_1} \sqrt{X_1^2 + Y_1^2} \tag{25}$$

$$\phi-\theta = \tan^{-1} (\frac{Y_1}{X_1}) . \tag{26}$$

With reverse rotation:

$$n_1 = \frac{2}{AT_2} \sqrt{X_2^2 + Y_2^2} \tag{27}$$

$$\phi+\theta = -\tan^{-1} (\frac{Y_2}{X_2}) . \tag{28}$$

It is to be noted that the angles in the forward and reverse directions differ by the sign on θ, thus the average of the two values yields ϕ. The value of n_1 is seen to be identical in both the forward and reverse directions. When ϕ and n_1 are known, the transfer function is determined.

II. LITERATURE SURVEY

Since the objective of this investigation is to study the measurement of the reactor transfer function by means of oscillator techniques, a review of the literature related to transfer function measurements in nuclear reactors is presented. Also work related to coupled-core reactor kinetics is briefly described.

A general theory of coupled-core reactors was introduced by Avery [2]. He used a point-kinetics equation for each core which includes coupling terms to account for the diffusion of neutrons from core to core. A similar technique was proposed by Baldwin [4] who used a one-group diffusion equation to simplify the coupled-reactors kinetic equations and develop the transfer function. Hansen [14] has generalized the theory of coupled-reactors by deriving a set of equations starting from the transport equation. Other work relating to coupled-core reactors has been reported [8, 21, 25].

The first reported transfer function measurements were made by Harrer et al. [16] on the CP-2. They used a cadmium oscillator located at the center of the core. The reactivity was varied sinusoidally with time by oscillating the cadmium rod. Experimental data were obtained at discrete frequencies. Good agreement was obtained with their point kinetics model at the low frequencies ($\leq$ 20 rad/sec) investigated.

Lundholm et al. [17] utilized both reactor oscillator

techniques and power spectral density measurements to in-
vestigate the SRE transfer function. Both methods were found
to be consistent with theory within experimental accuracy.
They found [13] that the oscillation technique is better
suited for the reactor where the prompt lifetime corner
frequency is less than 5 Hz and noise analysis is more
suitable for reactors with corner frequencies above 20 Hz.

DeShong [10] measured the frequency response of EBWR by
means of a sinusoidal reactivity variation method. He found
a resonance phenomenon occurring at high frequencies. The
height of the resonance and bandwidth at the half-power points
is a function of power, pressure, and temperature. A linear-
ized feedback model that describes this phenomenon has been
presented by Thie [27]. The model is composed of the zero
power reactor transfer function modified by two feedback
paths, one due to power generated in the boiling zone, the
other caused by boiling boundary fluctuations due to power
generated in the nonboiling zone.

Many other papers on transfer function measurements and
analysis have been reported [7, 12, 26] and these investiga-
tions are summarized in text books [15, 24].

The application of noise-analysis methods to reactor
kinetic studies was developed soon after Moore [19] combined
the theories of stochastic processes and reactor kinetics.
He pointed out that the noise spectrum of a stochastic system,

i.e. the mean square noise amplitude per unit bandwidth, is proportional to the square modulus of the transfer function and to the Fourier cosine transform of the auto-correlation function. The advantage of using this technique is that the information about transfer functions obtained from the noise is least subject to non-linear distortion.

Using a tunable band-pass filter, Cohn [6] measured the mean square noise amplitude of several low-power experimental facilities at Argonne National Laboratory. In order for the experiments to give meaningful results, the "pile noise component" in the chamber output must be large compared to the "white noise component" resulting from the statistics of neutron capture. He used a chamber heavily loaded with boron and placed in a high flux region in the reactor. Finally, the equipment was calibrated by exposing the chamber to white noise in the form of a large Co-60 source.

Balcomb et al. [3] employed cross-correlation techniques to measure the impulse response of Kiwi-A3. A small transfer tube through the reactor center was used to produce controlled perturbations which preserved the system linearity. This input and the reactor output were cross-correlated. Since the cross-correlation function is proportional to the impulsive response of the reactor for this type of input, the reactor transfer function is obtained from the Laplace transformation of the impulsive response. The main advantages of the method proposed

by them are (1) the entire information about the impulse response of the system is obtained in a short time, (2) small input amplitude perturbation are used so it is not hazardous, (3) the measurements can be used in the presence of strong noise sources.

Rajagopal [22] used analog correlation techniques to determine the transfer function for a small reactor at Brookhaven National Laboratory. A cadmium absorber located in the reactor was driven by random pulses obtained from a detector observing a radioactive source. This random external reactivity input produced by the cadmium absorber was cross-correlated with the system output. The results show that the measured transfer function agrees with the calculated transfer function.

Harrer mentioned in his book [15] that the techniques of cross-correlation were very useful in extracting a meaningful signal from a noise signal background. He suggested that the signal from the flux measurement ion chamber be cross-correlated with sin-cos functions which come from a sin-cos potentiometer which is coupled to the oscillator. Two outputs were used to obtain the amplitude and phase.

Recently Engen [11] followed Harrer's method to measure the open loop and closed loop transfer functions of EBR-II. Also he utilized the rod-drop technique to determine the reactor feedback system. The rod-drop method was performed

with a special stainless steel control rod. It was dropped out of the core to cause a power decrease, and the system reactivity was computed. Both methods were compared and it was shown that the rod-drop technique has sufficient promise to warrant its continued use, particularly for feedback analysis at high power levels, where the oscillation mechanism suffered restrictions on its operation.

Several other papers using noise-analysis techniques such as auto- and cross-correlations as well as power and cross spectral densities are presented in the Symposium on Noise Analysis in Nuclear Systems [28]. A good studies and detailed descriptions of measuring reactor noise have been summarized in a book by Thie [27].

The frequency response measurements performed up to date at Iowa State University were made above 10^{-1} Hz and the reactor was operated without the control system [18]. The present study is the first investigation conducted on the UTR-10 reactor which involves closed loop and low frequency measurements.

III. EXPERIMENTAL EQUIPMENT

A. Reactor

The experiments were carried out in the Iowa State University UTR-10 reactor. The UTR-10 [1] is a 10 KW heterogeneous, light water moderated, graphite reflected, thermal reactor designed as a teaching and research reactor. The reactor core consists of two 5 in. by 20 in. by 24 in. subcores separated by 18 in. of graphite and reflected by 12 in. of graphite. Each subcore contains approximately 72 MTR-type fuel plates. Five removable graphite stringers are provided in the reflector region between the subcores. One of the stringers is 4 in. by 4 in. by 48 in. long and is located at the center of the core where the oscillator was placed. A 4 ft. by 5 ft. by 5 ft. long thermal column containing 15 stringers is also provided. The central thermal column stringer involves two pieces of graphite, the outer one is 4 in. by 4 in. by 50 in. long, the inner one is 19.5 in. long. These two pieces of graphite were taken out when the ion chamber was inserted.

The uranium enriched to 93% or greater in U-235 is contained as $U Al_4$ solid solution in aluminum. This matrix is clad with 80 mils of aluminum, metallurically bonded to the fuel region. The maximum thermal neutron flux at full power is approximately 2×10^{11} neutrons/cm^2-sec.

The reactor is controlled by varying the vertical position

of neutron-absorbing control rods located in the reflector
adjacent to the core tank. Four control rods are provided;
one regulating rod, one shim-safety rod, and two safety rods.
The reactor flux is controlled by positioning the regulating
and shim-safety rods in the reflector from the control console.
The safety rods are fully withdrawn during normal operation.

The top view of the UTR-10 core is shown in Figure 5.
Figure 6 shows the ion chamber inserted in the thermal column.

B.   Reactivity Oscillator

The reactivity oscillator used in this experiment is
a 6.5 ft. long rectangular parallelepiped as shown in Figure
7. It consists of four major components.

The first and the most important component is the
reactivity oscillation generator. It has two suitably shaped
pieces of cadmium mounted on the stator and rotor. The station-
ary cadmium (stator) is a small rectangle of 20 mils and is ro-
tated by the rotor which has a petal shape (Figure 8) whose
analytical form in polar coordinates is

$$r^2 = K \cos \theta \qquad -\frac{\pi}{2} \le \theta \le \frac{\pi}{2} \; .$$

The sinusoidal reactivity input obtained from this shape
is approximately of the form

$$\rho = -A + B \sin \omega t \; .$$

Figure 5. The top view of the UTR-10 core

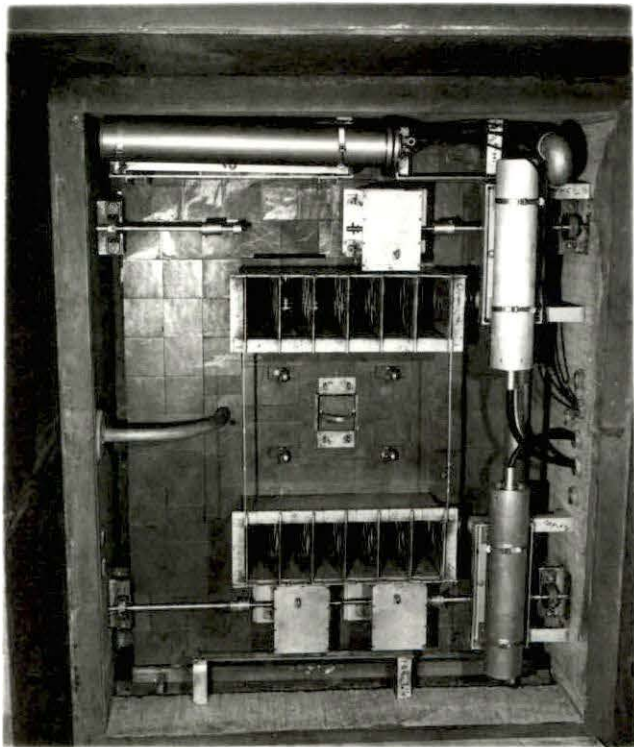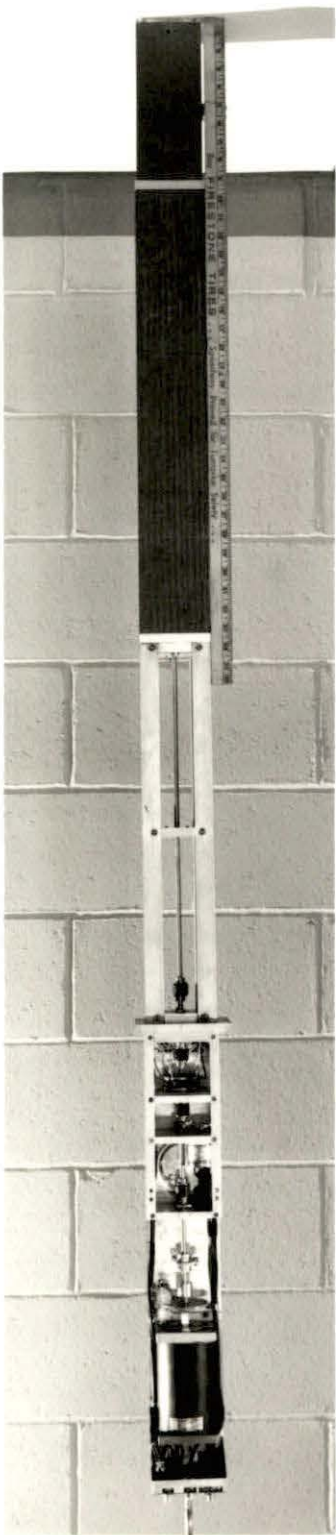Figure 6. The ion chamber inserted in the thermal column

Figure 7. The reactor oscillator

The actual reactivity variation of this oscillator has a static reactivity worth in its mean position of 8.1×10^{-4} and a sinusoidal oscillation amplitude of 2.0×10^{-4}. The reactivity worth measurement of the oscillator will be described in Section IV.

The second component is a speed reducer. When the oscillator is driven by the motor, a high rotational speed is obtained which is not suitable for low frequency measurements. By means of two speed reducers, 20:1 and 500:1, the frequency range from 600 rad/sec to 0.001 rad/sec is obtained. This range covers two break frequencies 46.8 rad/sec and 0.08 rad/sec which correspond to β/ℓ and $\overline{\lambda}$, respectively.

The third component consists of the disk, light source and photodiode. There are 50 equal-spaced holes in the disk. When the disk rotates with the oscillator, the light from the light source passes through these holes to the photodiode. The output from the photodiode is a series of pulses, the period of which is related to the motor speed. These pulses are applied to a feedback circuit to keep the motor speed uniform at the selected value.

The fourth component is the sin-cos potentiometer which is coupled to the oscillator to produce sin-cos functions having the same frequency as the oscillator. These sin-cos functions are sent to an analog computer for the cross-correlation calculations.
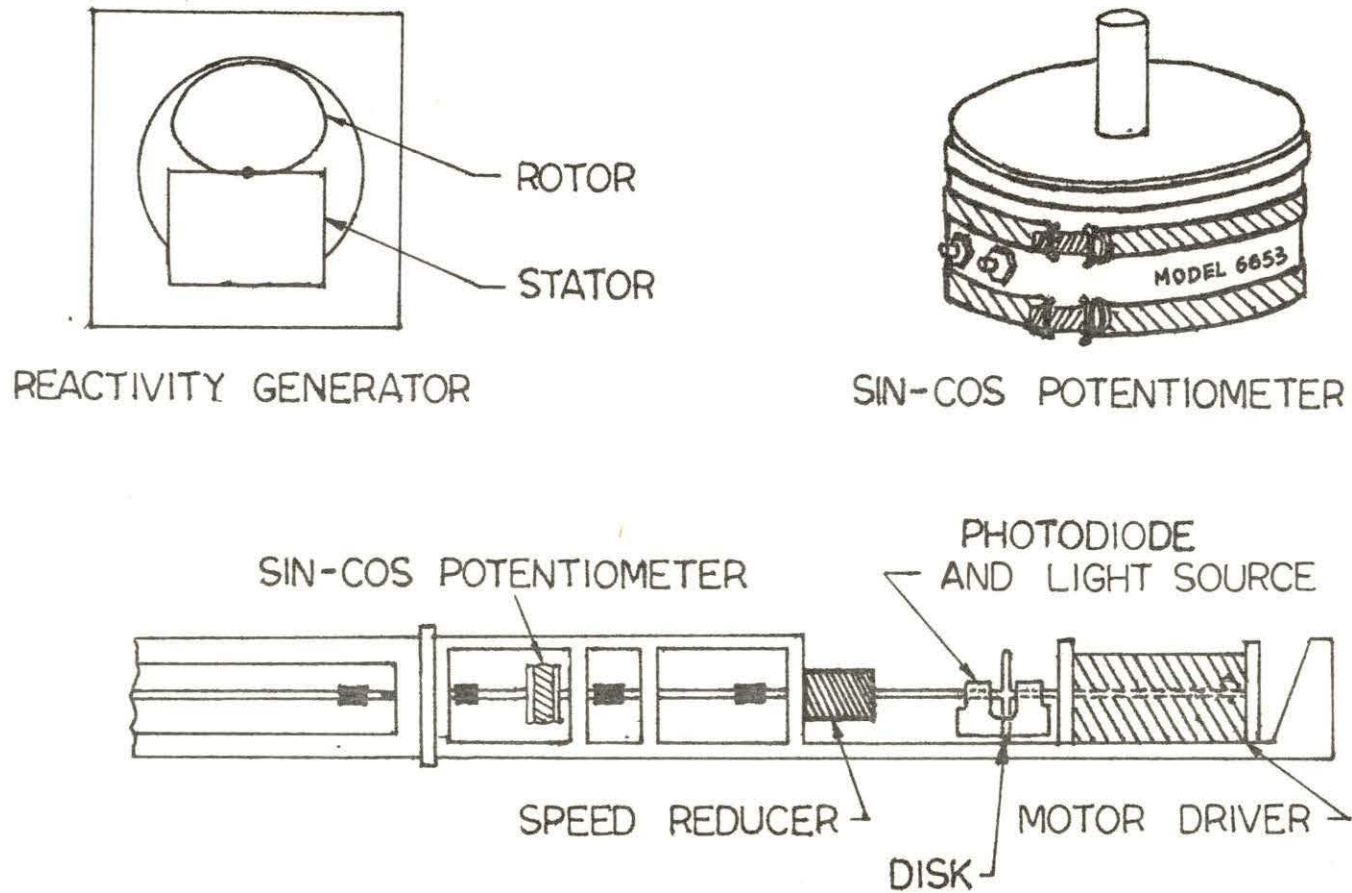
ROTOR

STATOR

REACTIVITY GENERATOR

MODEL 6653

SIN-COS POTENTIOMETER

SIN-COS POTENTIOMETER

PHOTODIODE
AND LIGHT SOURCE

SPEED REDUCER

DISK

MOTOR DRIVER

FIGURE 8. MAJOR COMPONENTS OF THE OSCILLATOR

Figure 8 shows the major components of the oscillator.

C.   Signal Measurement
Equipment

Basically the experimental methods used in this investigation involved the following steps: (1) the output current of the ion chamber, positioned inside the thermal column, was fed to a high speed picoammeter; (2) the d.c. current was bucked out to remove the steady state component by properly adjusting the current suppression dials on the picoammeter; and (3) the cross-correlation technique was carried out by a desk-top computing system consisting of a digital logic computer (DES-30)[1] connected to an analog computer (TR-48).[1]

The reactor signal was detected by a Reuter-Stokes Model RSN-15A neutron sensitive ionization chamber. The operating voltage and compensating voltage were chosen as 600 volts and -60 volts, respectively, for all runs. Two Fluke Model 405B high voltage DC power supplies were used to supply these voltages.

The Keithley Model 417 high speed picoammeter was used to convert the current signal to a voltage signal and to buck out the steady state component. Since the full capabilities of the high-speed circuitry in the picoammeter are realized by minimizing external capacitance, usually introduced by

[1]The TR-48 analog computer and the DES-30 digital logic computer were manufactured by Electronic Associates, Inc.

long cable runs to the input, the cable between the ion chamber and the picoammeter was chosen as short as possible.

The output of the picoammeter and sin-cos functions from the sin-cos potentiometer were sent to the TR-48 analog computer where cross-correlation was carried out. The DES-30 logic unit was used to control the TR-48 and to insure that an exact number of cycles was obtained as pointed out in Section I.

The pulses generated by the speed control circuitry were counted by a scaler to determine the frequency of oscillation. The frequency of oscillation was also determined by observing the period of the pulses with an oscilloscope.

IV. EXPERIMENTAL PROCEDURES

A. Frequency Response of Equipment

In order to check the frequency response of the instruments, power spectral density measurements using the reactor as a "white" noise source were performed. It should be noted that reactor transfer function measurements were made using most of the instruments shown in Figure 9. The block diagram of the system used for these measurements is presented in Figure 9.

The following operations were performed:

(1) The reactor was operated at 100 watts and the ion chamber was inserted in the thermal column, located 52 in. from the south core. Measurements were made with the ion chamber, located 52 in. from the south core. Measurements were made with the ion chamber at various positions to verify that the measurements were not influenced by the noise spectrum of the reactor.

(2) The high cutoff and low cutoff frequency settings were adjusted to the desired value.

(3) The integral of the square of the signal containing frequency components fixed by the band-pass filter settings was determined. The power spectral density was then determined by dividing the digital voltmeter reading by the integration time and the bandwidth of the filter.
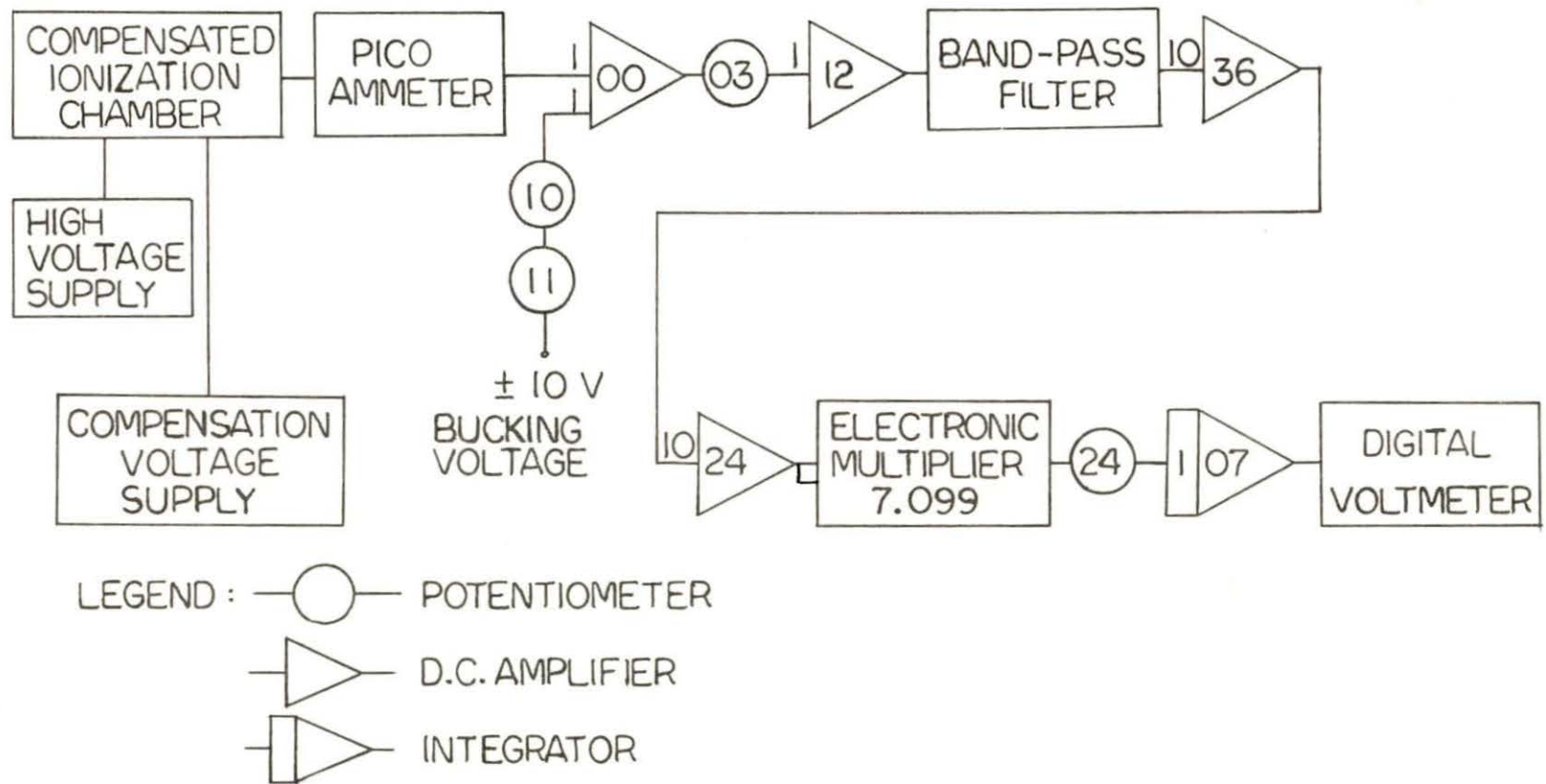
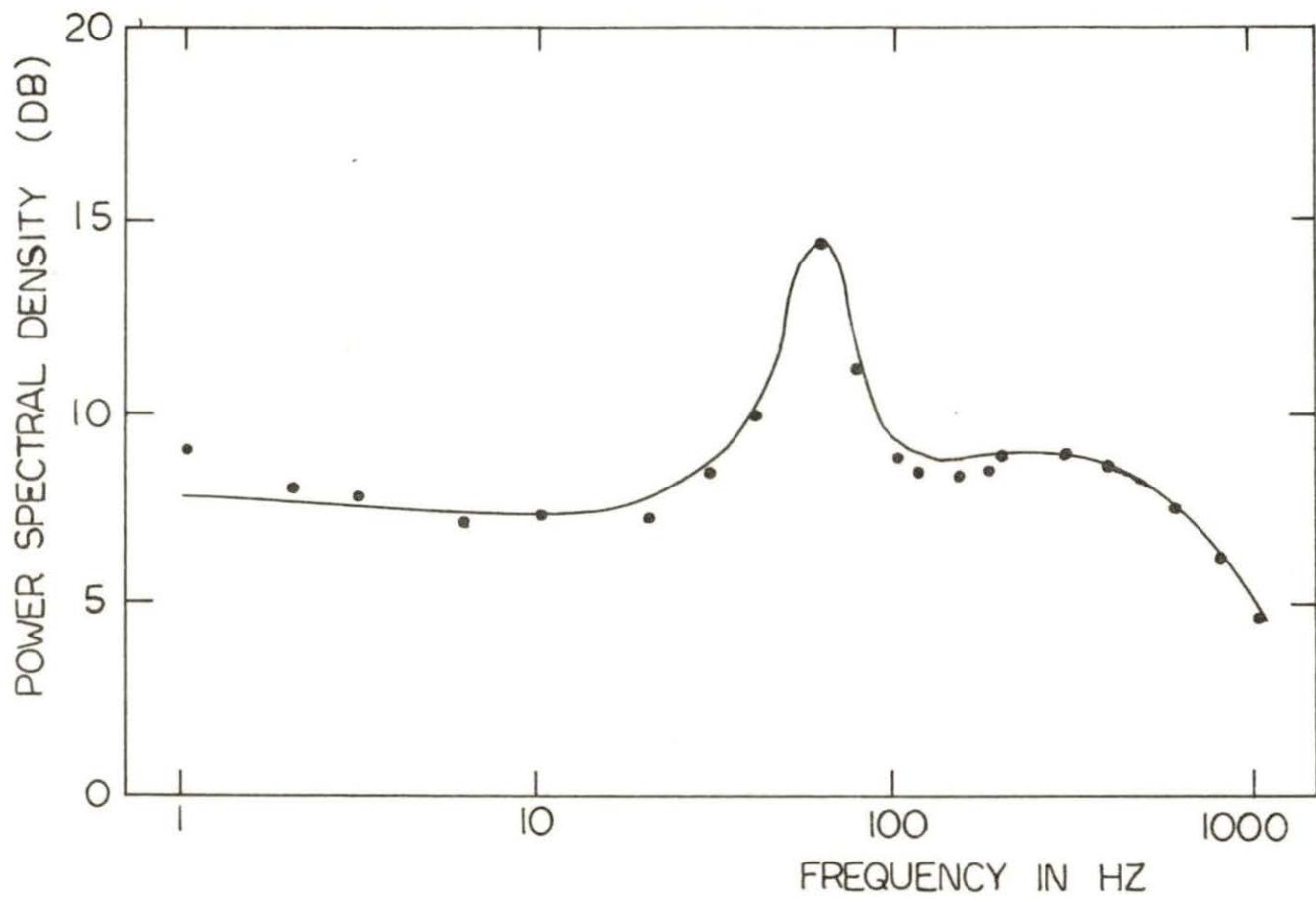FIGURE 9. BLOCK DIAGRAM FOR POWER SPECTRAL DENSITY MEASUREMENT

FIGURE 10. POWER SPECTRAL DENSITY OF WHITE NOISE FROM UTR-10

The bandwidth was assumed to be proportional to the midband frequency used on the bandpass filter.

The experimental results are given in Figure 10; where the power spectral density (in decibels) is plotted versus the midband frequency setting of the bandpass filter. The resulting curve is seen to be fairly constant (or uncorrelated) for $f \leq 20$ Hz. For $f > 20$ Hz there is a considerable peak occurring in the neighborhood of $f = 60$ Hz. This is interpreted as parastic 60 Hz noise from the power line. Thus it was concluded that the measuring system has a flat response out to at least 20 Hz.

B. Oscillator Reactivity Measurement

This section describes the procedures used to determine the static and dynamic "reactivity worth" of the reactor oscillator. This calibration was performed by inserting the oscillator in the reactor, in the location to be used during the experiment, and noting the critical regulating rod position as a function of the pattern position. The static reactivity worth of the oscillator was determined by comparing critical rod positions with and without the oscillator inserted in the reactor.

The measured oscillator reactivities were corrected for temperature change during the experiment. The water temperature at the reactor inlet and outlet were measured by
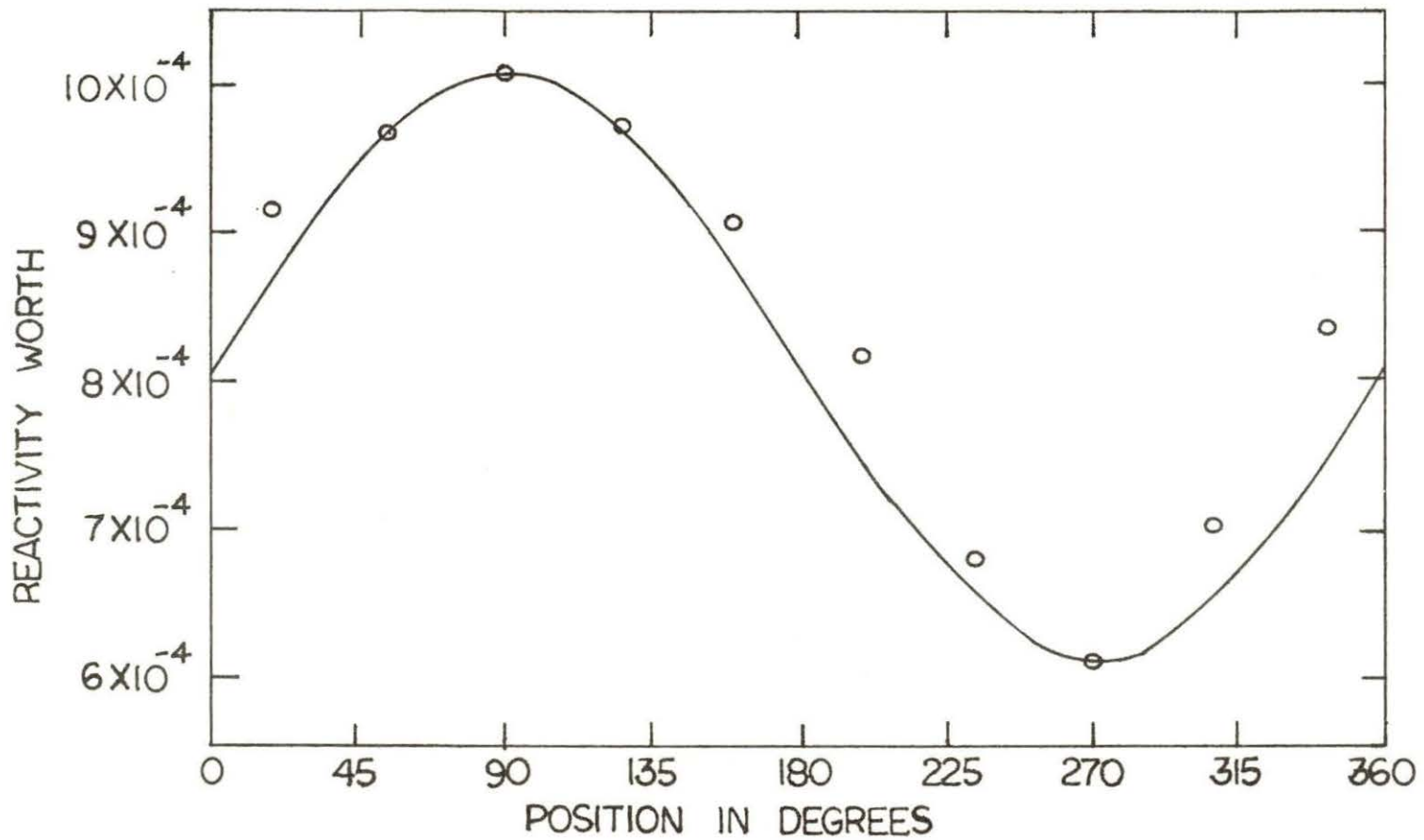
FIGURE 11. REACTIVITY WORTH OF OSCILLATOR WITH CADMIUM PATTERNS IN
VARIOUS POSITIONS

34

inserting thermocouples in the inlet and outlet pipes. From the reactor temperature coefficient, these temperatures were related to a reactivity change and then used to correct the oscillator reactivity.

The measured oscillator reactivities are given in Figure 11. This figure shows that the static reactivity worth (8.1×10^{-4}) is larger than the dynamic amplitude worth (2.0×10^{-4}) and the reactivity variations are approximately sinusoidal. An exact sinusoidal reactivity change is unnecessary since after the cross-correlation calculation only the fundamental mode remains.

C.   Transfer Function Measurement

The procedures used to perform the transfer function measurements are described in this section.

The oscillator was inserted in the center of the internal reflector and the ion chamber was positioned approximately 5 in. from the south core in the thermal column. The experimental setup is shown in Figure 12.

After the reactor was brought to the desired power level, 5 watts, the oscillator was switched on (in the forward direction). The rotation of the oscillator varied the neutron absorption rate cyclically, with the maximum absorption occurring with the rotor fully outside the stator, and the minimum absorption occurring, a half-cycle later, with the
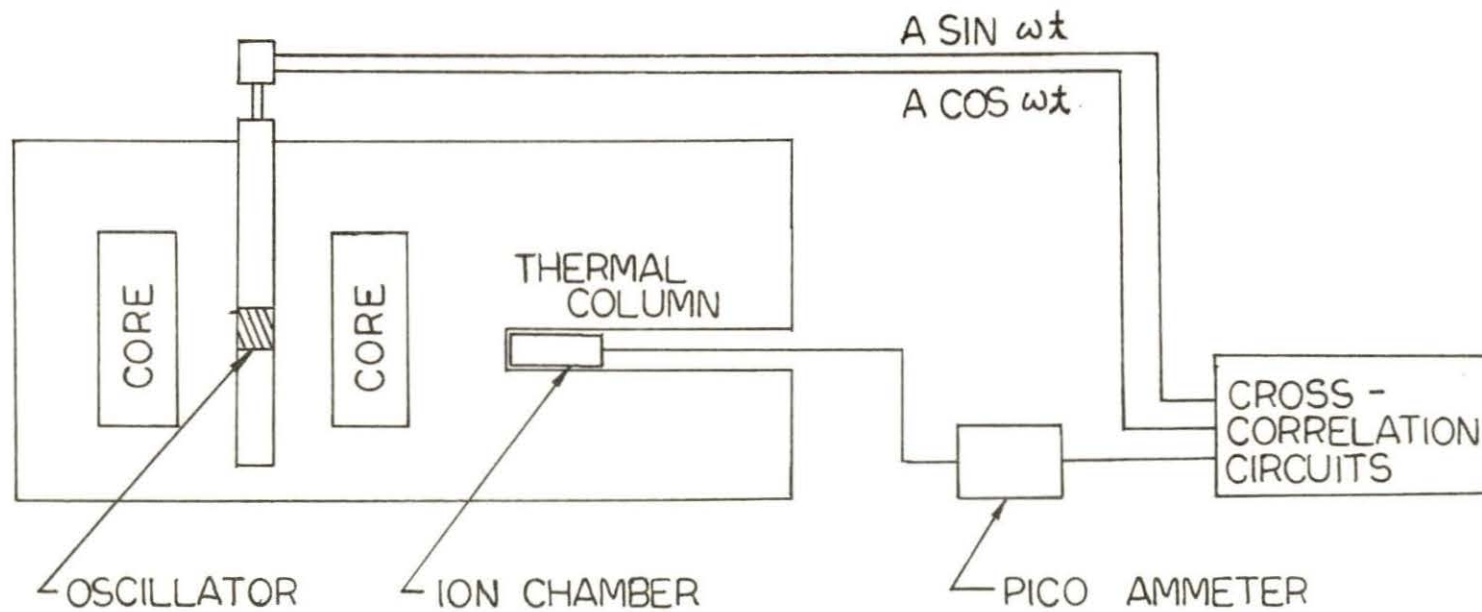
FIGURE 12. EXPERIMENTAL SETUP FOR MEASUREMENT OF THE UTR-10
FREQUENCY RESPONSE

rotor inside the stator. Operating the oscillator at constant
frequency and waiting until transient effects died out
produced an approximately sinusoidal flux changes.

The effect of the reactivity perturbation was seen by
connecting an oscilloscope to the output signal from the
picoammeter. This output signal and the sin-cos functions
generated by the sin-cos potentiometer coupled to the oscil-
lator were sent to the cross-correlation circuits. The
block diagram of this system is shown in Figure 13. The
numbers indicated in the potentiometer, d.c. amplifier, and
integrator are the networks used in this experiment. The
amplification gain is indicated in front of each network.

It should be noted that the undesirable steady state
components of the oscillator and detector signal were sup-
pressed before being sent to the cross-correlation circuit.
The suppression was carried out by properly adjusting the
current suppression dials on the picoammeter. In order to
have the noise signal and the steady state signal of the
reactor extracted completely, it is important to keep the
amplitudes of the output signal and the sin-cos functions
constant. The amplitudes of the sin-cos functions were set
at 10 volts to avoid TR-48 overloading. The amplitude of
the signal preceding the multiplications circuit was adjusted
to approximately 20 volts peak-to-peak by properly setting
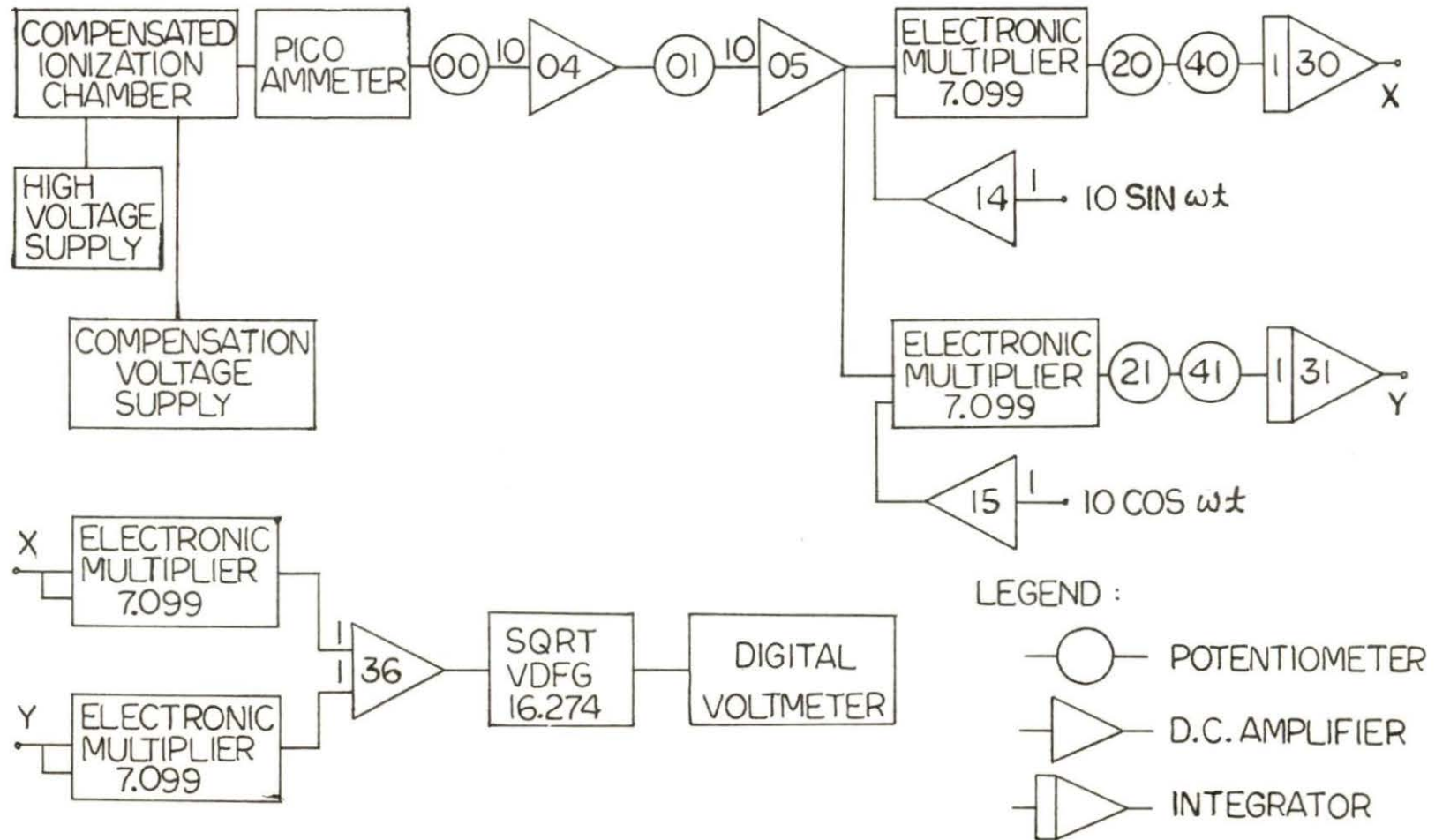the values of the potentiometers, 00 and 01. This adjustment

FIGURE 13. BLOCK DIAGRAM FOR TRANSFER FUNCTION MEASUREMENT

could be easily achieved by observing the signal into the multiplier on an oscilloscope. The input signals from the multipliers to the integrators were maintained as large as possible by manipulating the gains of the amplifiers and the potentiometers. For calculational convenience, the values of potentiometer 21 and 41 were set the same as those of 20 and 40. After integration, both signal, X and Y, were sent to squaring, summation, and square root circuits.

When an exact number of cycles was required in the low frequency range, the DES-30 was used with the TR-48. The logic circuit for controlling the TR-48 and measuring a complete number of cycles is presented in Figure 14. The operation of this logic circuit is described in Appendix B. When the number of cycles was set and the system was switched on, the logic circuit started to count the number of cycles produced by the oscillator and the transfer function measurement circuit was started. After the desired number of cycles was reached, the system was automatically stopped. For each set of data, picoammeter and potentiometer settings, amplifier gains, the integrated voltages, and the integration time were suitably recorded.

The measurements just described were repeated for the frequency range of 20 Hz to 0.006 Hz for both directions of the oscillator rotation. The open loop transfer function was obtained by operating the reactor on manual control during
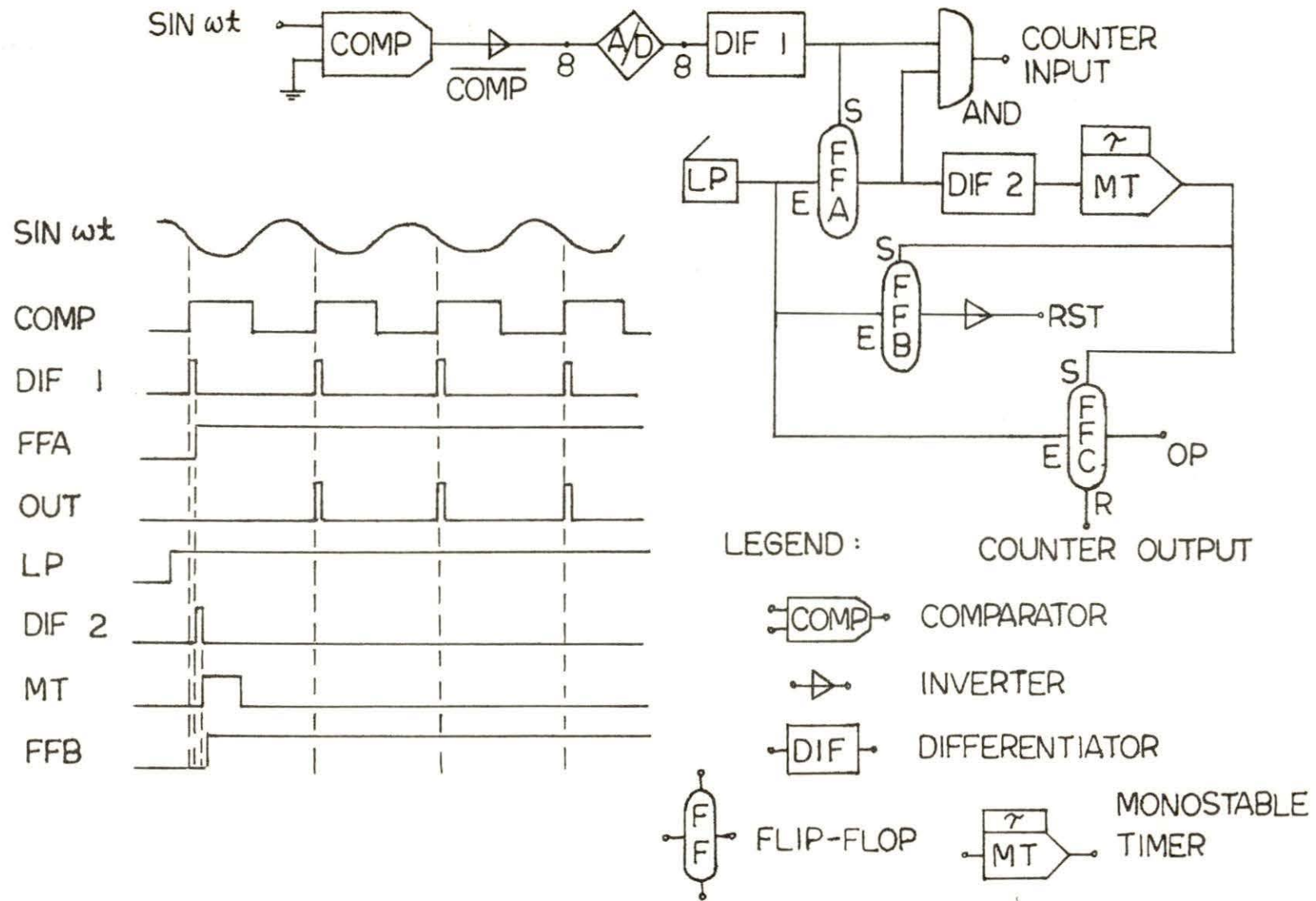
FIGURE 14. LOGIC CIRCUIT FOR MEASURING AN EXACT NUMBER OF CYCLES

the measurements. The closed loop transfer function was obtained by operating the reactor on automatic control. Since the sin-cos potentiometer was not moved during the low frequency measurements ($f \leq 3Hz$), the phase shift θ between the sin-cos potentiometer and the oscillator was measured from the open loop phase shift. According to Equation (26), the closed loop phase shift was then obtained by adding θ to the total phase shift obtained in the forward rotation.

The noise rejection capabilities of the cross-correlation system were checked by repeating several of the previous measurements with the oscillator operating outside the reactor.

D. Experimental Consideration

During the frequency response measurement, a number of possible sources of error can be reduced to a minimum value by following the procedures given below.

(1) The overloading of amplifiers (output above 10 volts) results in their saturation and introduces significant errors in the cross-correlation calculations. Overloading may be caused by a rather large amplification of signal voltage. A judicious control of circuit potentiometer settings eliminated this source of error.

(2) Since the error due to a non-integer number of cycles is inversely proportional to the frequency (Equations (40) and (42)), the use of an exact number of cycles is

important at low frequencies. The DES-30 digital
logic computer was used at low frequencies for this
purpose.

(3) If the input signal to the multiplier has a steady state
component and a non-integer number of cycles is used,
serious errors can result. In practice, this steady
state component was suppressed by the picoammeter and
there was no drift in this component after the initial
adjustment if the reactor power level was kept constant.

(4) It is important that the oscillator frequency remains
constant during a measurement. Non-uniform oscillation
will produce non-exact sin-cos functions from the sin-
cos potentiometer. Significant error is then intro-
duced in the data. This source of error was eliminated
by starting measurement after the transient oscillation
died out.

(5) In order to have the noise signal and steady state signal
of the reactor extracted completely, it was important
to keep the amplitude of the output signal and the sin-
cos functions constant.

(6) The output signal from the ion chamber always has some
noise associated with it which is caused by statistical
fluctuations in the arrival of neutrons at the ion
chamber. The signal-to-noise ratio is poor when the
reactor power level is low and/or the ion chamber is

located far from the core. Although the cross-correlation technique yields precise results with a poor signal-to-noise ratio, this requires integration over a large number of cycles as the ratio becomes poorer. Rather low signal-to-noise ratio was avoided as far as possible.

(7) The full capabilities of the high-speed circuitry in the picoammeter are realized by minimizing external capacitance, usually introduced by long cable runs to the input, the cable between the ion chamber and the picoammeter was chosen as short as possible.

E. Data Analysis

In order to obtain more accurate results, data analysis was carried out with the IBM-360 computer using programs written in the FORTRAN language. Since the computer sub-routine for the arctangent gives angles from 0 to plus π for positive arguments and angles from 0 to minus π for negative arguments, according to Equations (26) and (28) there is no problem in obtaining the correct open loop phase angle if the sign is changed in reverse rotation. For the closed loop phase angle, a correction was made.

It was assumed that π should be subtracted from each phase angle in the feedback (or closed loop) measurements. This assumption proved to be valid.

Table 1 summarizes the program tests of the sign of
the numerator Y and denominator X of the arctangent argument.
The table also indicates the equations to be used in the
computation.

Table I. Program tests for correct phase angle computation

Algebraic sign of Y	Algebraic sign of X	Equation to be used
+	+	(29)
+	-	(29)
-	+	(30)
-	-	(30)

The equations referred to in Table I are as follows:

$$\phi - \theta = \tan^{-1} (Y/X) - \pi \tag{29}$$

$$\phi - \theta = \tan^{-1} (Y/X) + \pi \tag{30}$$

As for the amplitude, both open loop and closed loop
were calculated by Equations (25) and (27) and normalized
by the normalization factor which included picoammeter set-
ting, potentiometer setting, and integration time.

The FORTRAN programs for both the open loop and closed
loop are shown in Appendix C and the experimental results are
shown in Appendix D. The standard deviations for several
frequencies are also provided in Appendix D. The notations
GMAG, GDB, PHRAD, and PHDEG in the output denote gain

(relative magnitude), gain (DB), phase angle (radian), and phase angle (degree), respectively, and the notation CONV in the program denotes the normalization factor, M is the input data sets.

It should be noted that during the entire experiment an exact number of cycles was taken below 3 Hz and above 3 Hz a fixed integration time (60 sec) method was used. The error resulting from non-integral cycles is presented.

From Equation (9), if K is non-integer, it becomes

$$\Psi_{fg}(0) = \frac{fA}{K}[\int_0^{K/f} N(t) \sin\omega t \, dt + \int_0^{K/f} n_0 \sin\omega t \, dt$$

$$+ \int_0^{K/f} n_1 \sin(\omega t + \phi) \sin\omega t \, dt]$$

$$= \frac{fA}{K} [\int_0^{K/f} N(t) \sin\omega t \, dt + \frac{n_0}{\omega} (1 - \cos\frac{K\omega}{f})$$

$$+ \frac{n_1}{\omega} \cos\phi(\frac{K\omega}{2f} - \frac{1}{4}\sin\frac{2K\omega}{f}) + \frac{n_1}{2\omega} \sin\phi \sin^2\frac{K\omega}{f}] .$$

With $\omega = 2\pi f$, the above equation becomes

$$\Psi_{fg}(0) = \frac{fA}{K}[\int_0^{K/f} N(t) \sin 2\pi ft \, dt + \frac{n_0}{2\pi f} (1 - \cos 2\pi K)$$

$$+ \frac{n_1}{2\pi f} \cos\phi(\pi K - \frac{1}{4}\sin 4\pi K) + \frac{n_1}{4\pi f} \sin\phi \sin^2 2\pi K]$$

$$= \frac{An_1}{2} \cos\phi - \frac{An_1}{8\pi K} \cos\phi \sin 4\pi K + \frac{An_1}{4\pi K} \sin\phi \sin^2 2\pi K$$

$$+ \frac{An_0}{2\pi K} (1 - \cos 2\pi K) + \frac{fA}{K} \int_0^{K/f} N(t) \sin 2\pi ft \, dt. \quad (31)$$

In a similar way, for non-integer K, Equation (12) becomes

$$\Psi_{fg}(1/4f) = \frac{An_1}{2} \sin\phi + \frac{An_1}{8\pi K} \sin\phi \sin 4\pi K + \frac{An_1}{4\pi K} \cos\phi \sin^2 2\pi K$$

$$+ \frac{An_0}{2\pi K} \sin 2\pi K + \frac{fA}{K} \int_0^{K/f} N(t) \cos 2\pi ft \; dt \; . \quad (32)$$

From Equations (31) and (32), define

$$X = \frac{An_1}{2} \cos\phi \qquad\qquad\qquad\qquad\qquad\qquad (33)$$

$$\Delta X = -\frac{An_1}{8\pi K} \cos\phi \sin 4\pi K + \frac{An_1}{4\pi K} \sin\phi \sin^2 2\pi K$$

$$+ \frac{An_0}{2\pi K} (1-\cos 2\pi K) + \frac{fA}{K} \int_0^{K/f} N(t) \sin 2\pi ft \; dt \qquad (34)$$

$$Y = \frac{An_1}{2} \sin\phi \qquad\qquad\qquad\qquad\qquad\qquad (35)$$

$$\Delta Y = \frac{An_1}{8\pi K} \sin\phi \sin 4\pi K + \frac{An_1}{4\pi K} \cos\phi \sin^2 2\pi K$$

$$+ \frac{An_0}{2\pi K} \sin 2\pi K + \frac{fA}{K} \int_0^{K/f} N(t) \cos 2\pi ft \; dt. \qquad (36)$$

Since the steady state component n_0 was suppressed by the pico-ammeter to a very small value compared with n_1 and if the noise signal $N(t)$ is assumed to be small, both the third and the fourth terms in Equations (34) and (36) may be neglected, with the result

$$\Delta X \approx - \frac{An_1}{8\pi K} \cos\phi \sin 4\pi K + \frac{An_1}{4\pi K} \sin\phi \sin^2 2\pi K$$

$$\leq \frac{An_1}{8\pi K} + \frac{An_1}{4\pi K}$$

$$= \frac{3An_1}{8\pi K} \tag{37}$$

$$\Delta Y \approx \frac{An_1}{8\pi K} \sin\phi \sin 4\pi K + \frac{An_1}{4\pi K} \cos\phi \sin^2 2\pi K$$

$$\leq \frac{An_1}{8\pi K} + \frac{An_1}{4\pi K}$$

$$= \frac{3An_1}{8\pi K} \quad . \tag{38}$$

The error, E_m, in the magnitude due to non-integer K is given by

$$E_m = \sqrt{(X+\Delta X)^2 + (Y+\Delta Y)^2} - \sqrt{X^2+Y^2}$$

$$= \sqrt{X^2+Y^2+2(X\Delta X+Y\Delta Y)+(\Delta X)^2+(\Delta Y)^2} - \sqrt{X^2+Y^2}$$

$$= \sqrt{(\frac{An_1}{2})^2 + \frac{3(An_1)^2}{8\pi K}(\sin\phi+\cos\phi) + 2(\frac{3An_1}{8\pi K})^2} - \sqrt{(\frac{An_1}{2})^2}$$

$$= \frac{An_1}{2} \left[\sqrt{1 + \frac{3}{2\pi K}(\sin\phi+\cos\phi)+2(\frac{3}{4\pi K})^2} - 1 \right] \quad . \tag{39}$$

Normalizing E_m by dividing E_m by the amplitude, $G(= \frac{An_1}{2})$, yields

$$\frac{E_m}{G} = \sqrt{1 + \frac{3}{2\pi K}(\sin\phi+\cos\phi)+2(\frac{3}{4\pi K})^2} - 1$$

$$\leq \sqrt{1 + \frac{3}{2\pi K} \cdot \sqrt{2} + (\frac{3\sqrt{2}}{4\pi K})^2} - 1$$

$$= \frac{3\sqrt{2}}{4\pi K} . \tag{40}$$

The phase error, E_ϕ, due to non-integer K is given by

$$E_\phi = \tan^{-1}(\frac{Y+\Delta Y}{X+\Delta X}) - \tan^{-1}(\frac{Y}{X})$$

$$\tan E_\phi = \tan[\tan^{-1}(\frac{Y+\Delta Y}{X+\Delta X}) - \tan^{-1}(\frac{Y}{X})]$$

$$= \frac{\frac{Y+\Delta Y}{X+\Delta X} - \frac{Y}{X}}{1 + \frac{Y+\Delta Y}{X+\Delta X} \cdot \frac{Y}{X}}$$

$$= \frac{X\Delta Y - Y\Delta X}{X^2 + Y^2 + X\Delta X + Y\Delta Y}$$

$$= \frac{\frac{3(An_1)^2}{16\pi K}(\cos\phi - \sin\phi)}{\frac{(An_1)^2}{4} + \frac{3(An_1)^2}{16\pi K}(\cos\phi + \sin\phi)}$$

$$= \frac{3(\cos\phi - \sin\phi)}{4\pi K + 3(\cos\phi + \sin\phi)} .$$

Assuming E_ϕ is very small, the above equation becomes

$$E_\phi \simeq \frac{3(\cos\phi - \sin\phi)}{4\pi K + 3(\cos\phi + \sin\phi)} . \tag{41}$$

For the worst case, when the numerator $3(\cos\phi - \sin\phi)$ is $3\sqrt{2}$ and the denominator is $4\pi K - 3\sqrt{2}$, Equation (41) becomes

$$E_\phi \leq \frac{3\sqrt{2}}{4\pi K - 3\sqrt{2}}$$

$$= \frac{3\sqrt{2}}{4\pi f T - 3\sqrt{2}} . \qquad (42)$$

For both results, Equations (40) and (42), it is evident that the longest integration times T will be needed for the lowest frequency f. In this experiment, 60 sec integration time was always used when the frequency was above 3 Hz. Table II shows these approximate estimates of the normalized error E_m/G and the phase angle error E_ϕ for different f with fixed integration time. Since the worst case is always considered in Equations (40) and (42), the actual experimental errors due to non-integer K are significantly smaller than the estimated errors.

Table II. Estimated errors due to non-integer K

f (Hz)	T (sec)	$\dfrac{E_m}{G} = \dfrac{3\sqrt{2}}{4\pi f T}$	$E_\phi = \dfrac{3\sqrt{2}}{4\pi f T - 3\sqrt{2}}$
3	60	0.187%	0.188
5	60	0.113%	0.113
10	60	0.056%	0.056
15	60	0.038%	0.038
20	60	0.028%	0.028

V. DISCUSSION AND RESULTS

The measured open loop and closed loop transfer functions
of the UTR-10 reactor are shown separately in Figures 15
through 18.

Figures 15 and 16 show the magnitude and phase shift
of the open loop transfer function both for the forward and
reverse directions of rotation of the oscillator. The phase
shift curve includes the error θ associated with the coupling
of the sin-cos potentiometer and the oscillator. This error
appears with opposite signs in the forward and reverse
directions and is consequently eliminated by taking the mean
value, which then represents the true phase response of the
reactor. The change in the error θ at 3 Hz was due to the
removal of the sin-cos potentiometer during the experiment.
To facilitate the comparison of experimental measurements
with the theoretical transfer function based on six delayed
neutron groups for a U-235 fueled thermal reactor [24]
results for two different neutron lifetimes are also pre-
sented in Figures 15 and 16. A coupled-core transfer function
is described in Appendix A.

For the closed loop transfer function, Figures 17 and 18
show the forward rotation of the oscillator. The true phase
response of the closed loop was obtained by adding θ, obtained
from the open loop, to the total phase shift obtained in
the forward rotation. The theoretical value of the closed loop
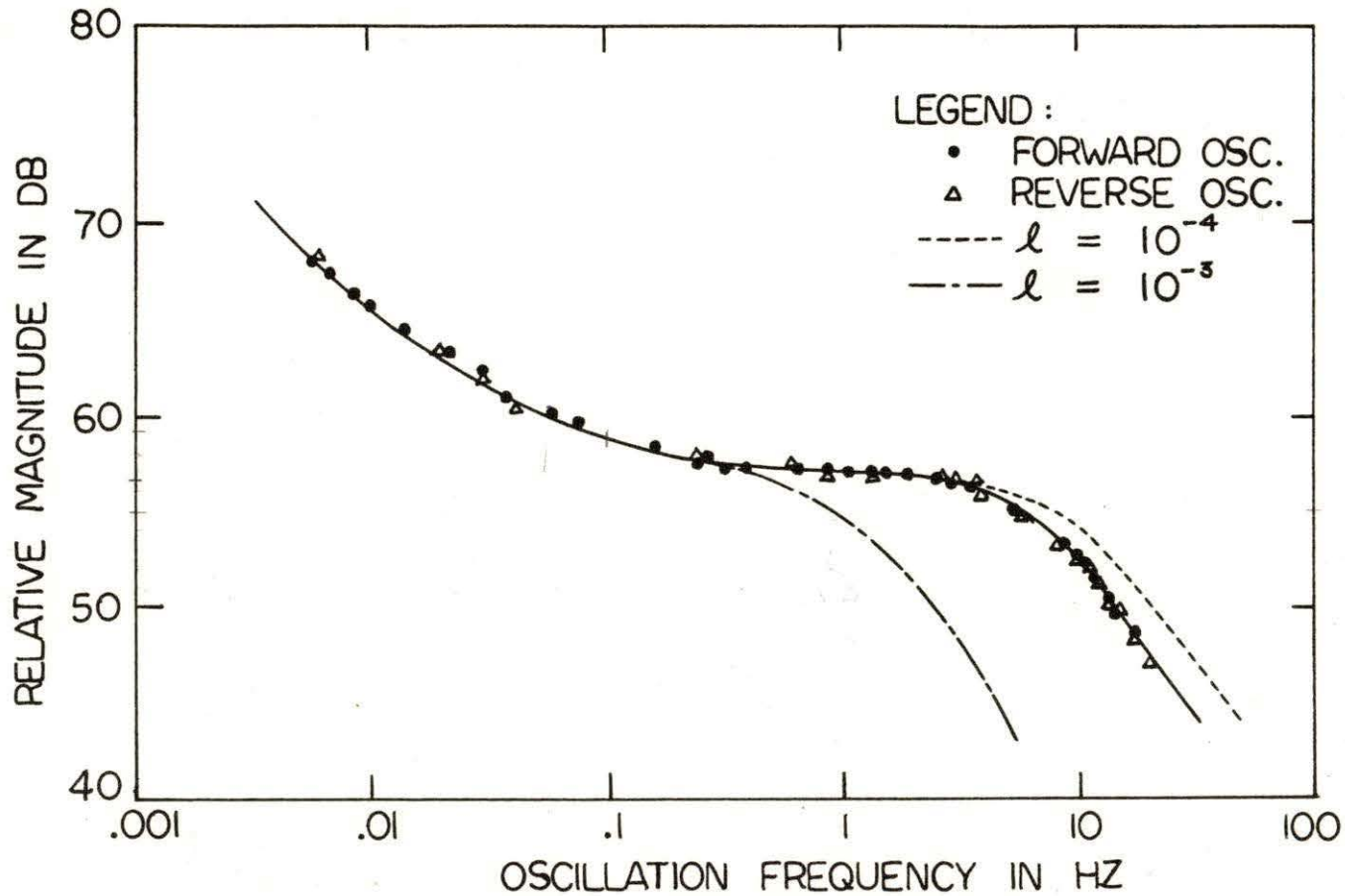transfer function based on the model in Figure 3 is given in

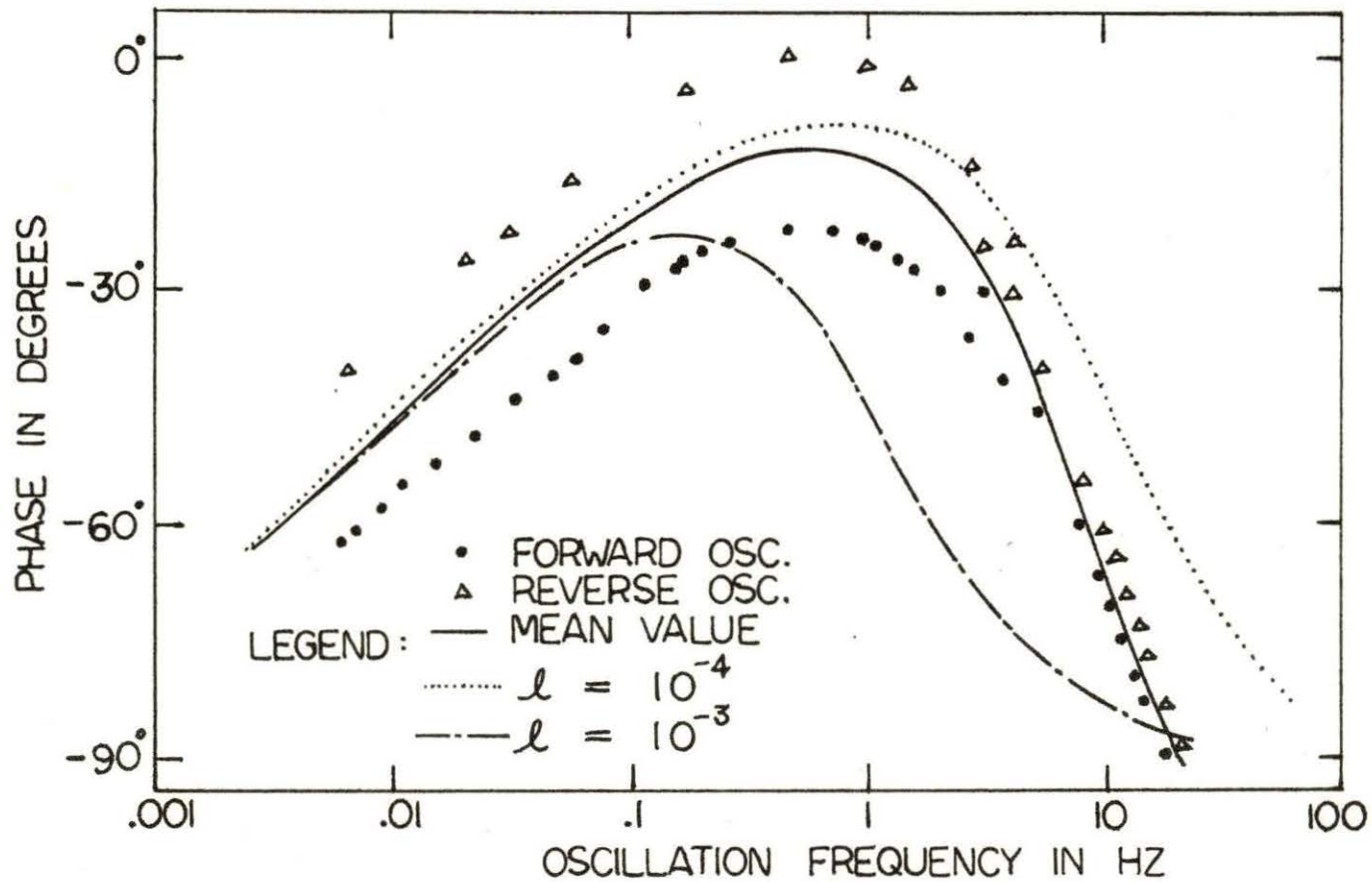FIGURE 15. MAGNITUDE OF THE OPEN LOOP TRANSFER FUNCTION

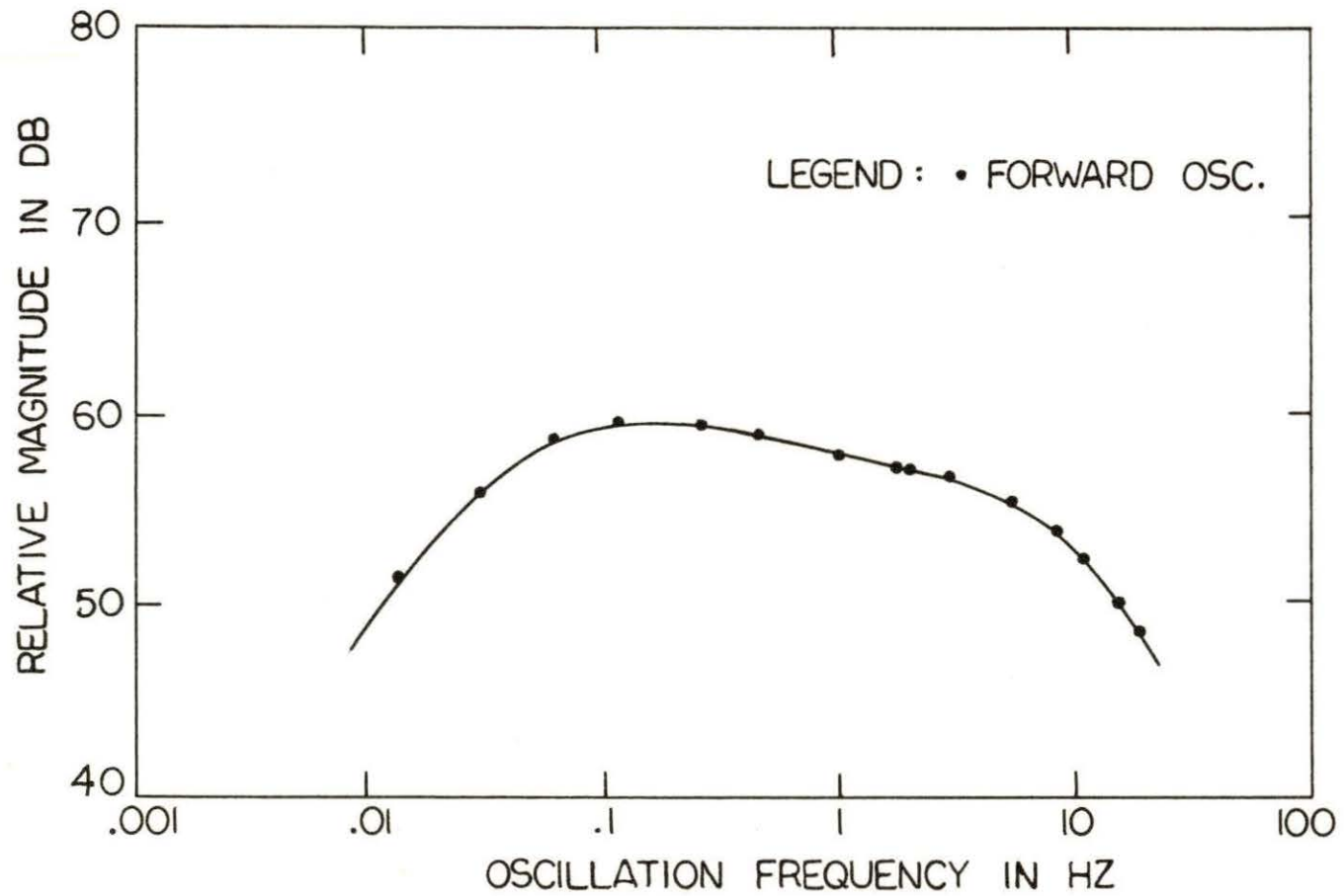FIGURE 16. PHASE ANGLE OF THE OPEN LOOP TRANSFER FUNCTION

FIGURE 17. MAGNITUDE OF THE CLOSED LOOP TRANSFER FUNCTION

53
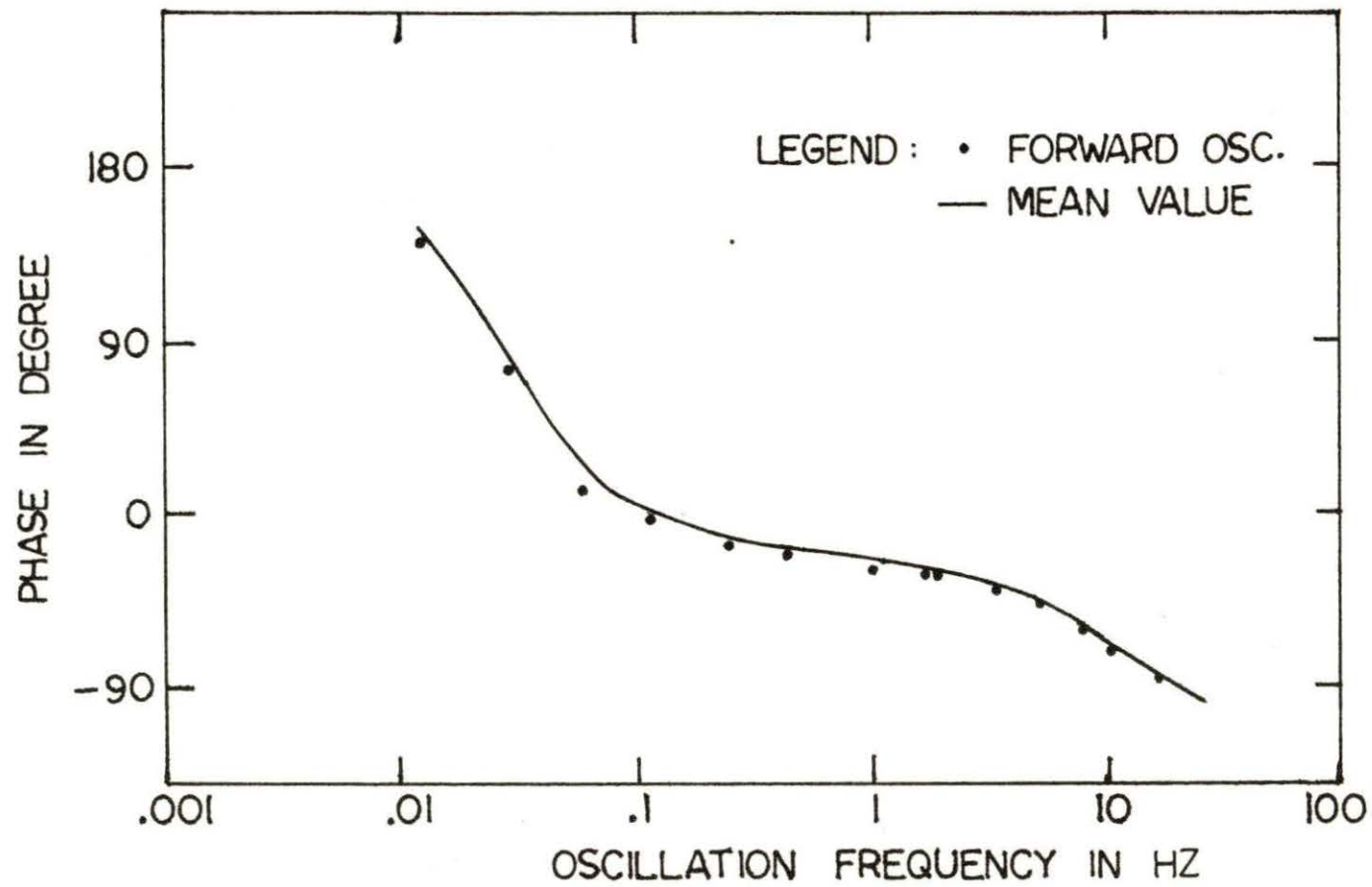
FIGURE 18. PHASE ANGLE OF THE CLOSED LOOP TRANSFER FUNCTION

Figures 19 through 22. The settings of αP%, I, and T in Figure 3 were chosen as 20, 1.0, and 8.2 for the experiment.

A study of Figures 15 through 18 reveals the following significant features of the experimental results:

(1) The neutron lifetime ℓ of the UTR-10 reactor is 1.35 x 10^{-4} sec and the two theoretical neutron lifetimes were 10^{-3} sec and 10^{-4} sec. Thus, at high frequencies, the experimental result of the open loop frequency response lies between the two theoretical values. The sharp decreasing phase shift, different from the theoretical smooth curves is thought to be due to the spatial dependence of the reactor response.

(2) At high frequencies, the magnitude is observed to drop off at 20 DB/decade and at low frequencies, good agreement is shown between experimental and theoretical results.

(3) Theoretical frequency response of the UTR-10 reactor obtained by the natural mode approximation [5] and the Green's function model approximation [20] show good agreement with the experimental result in the high frequency range $(f \geq 0.3$ Hz). No comparison was made in the low frequency range (f<0.3 Hz) however since the average decay constant $\overline{\lambda}$(=0.08 rad/sec) was used in both theoretical analyses.

(4) For the closed loop transfer function, theoretical values with different forward loop gains K, as shown in Figures

FIGURE 19. MAGNITUDE OF THEORETICAL CLOSED LOOP TRANSFER FUNCTION WITH I = 1.0 , T = 8.2 , α P% = 20
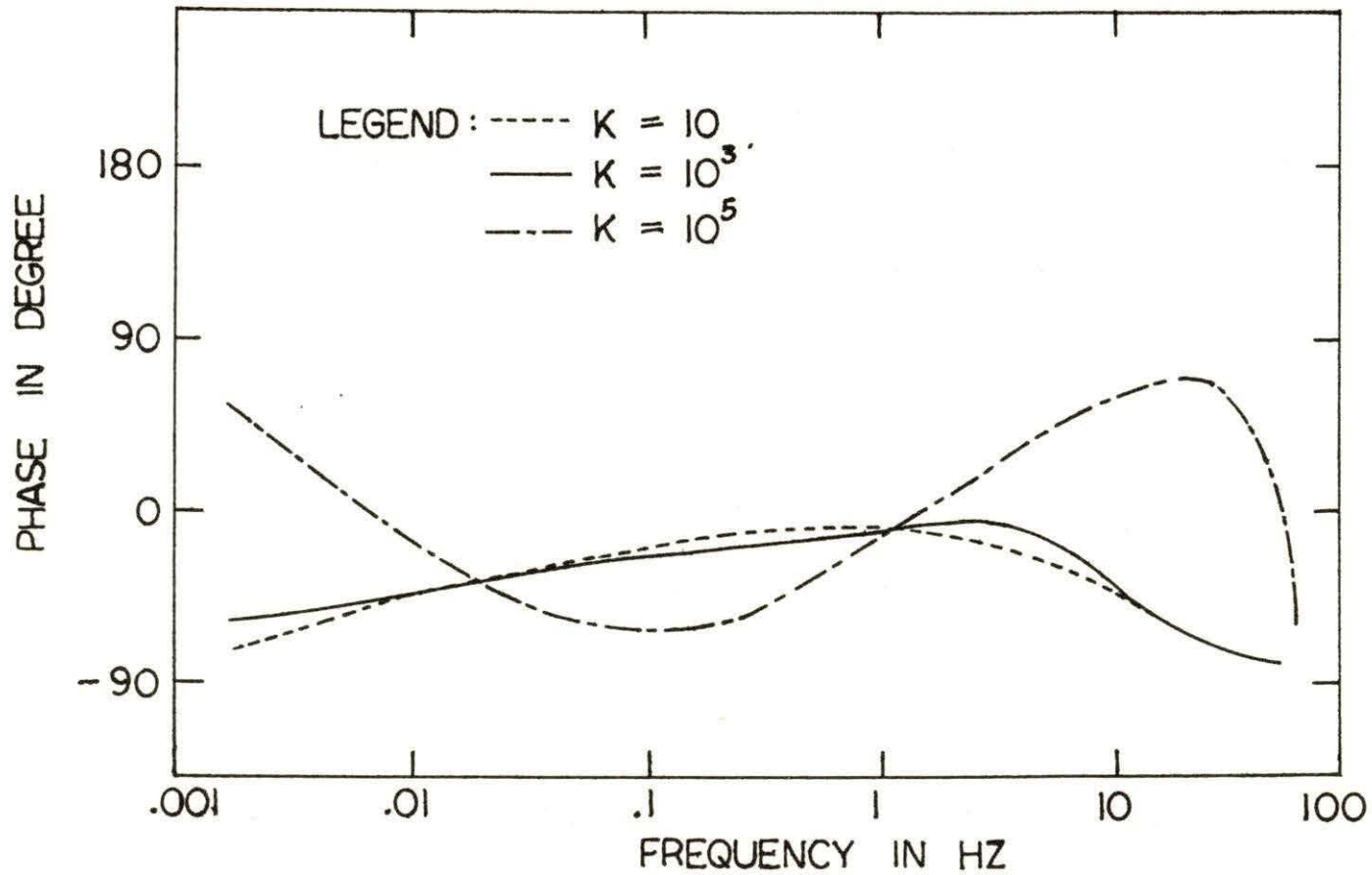
FIGURE 20. PHASE ANGLE OF THEORETICAL CLOSED LOOP TRANSFER
FUNCTION WITH I = 1.0 , T = 8.2 , $\alpha P \% = 20$
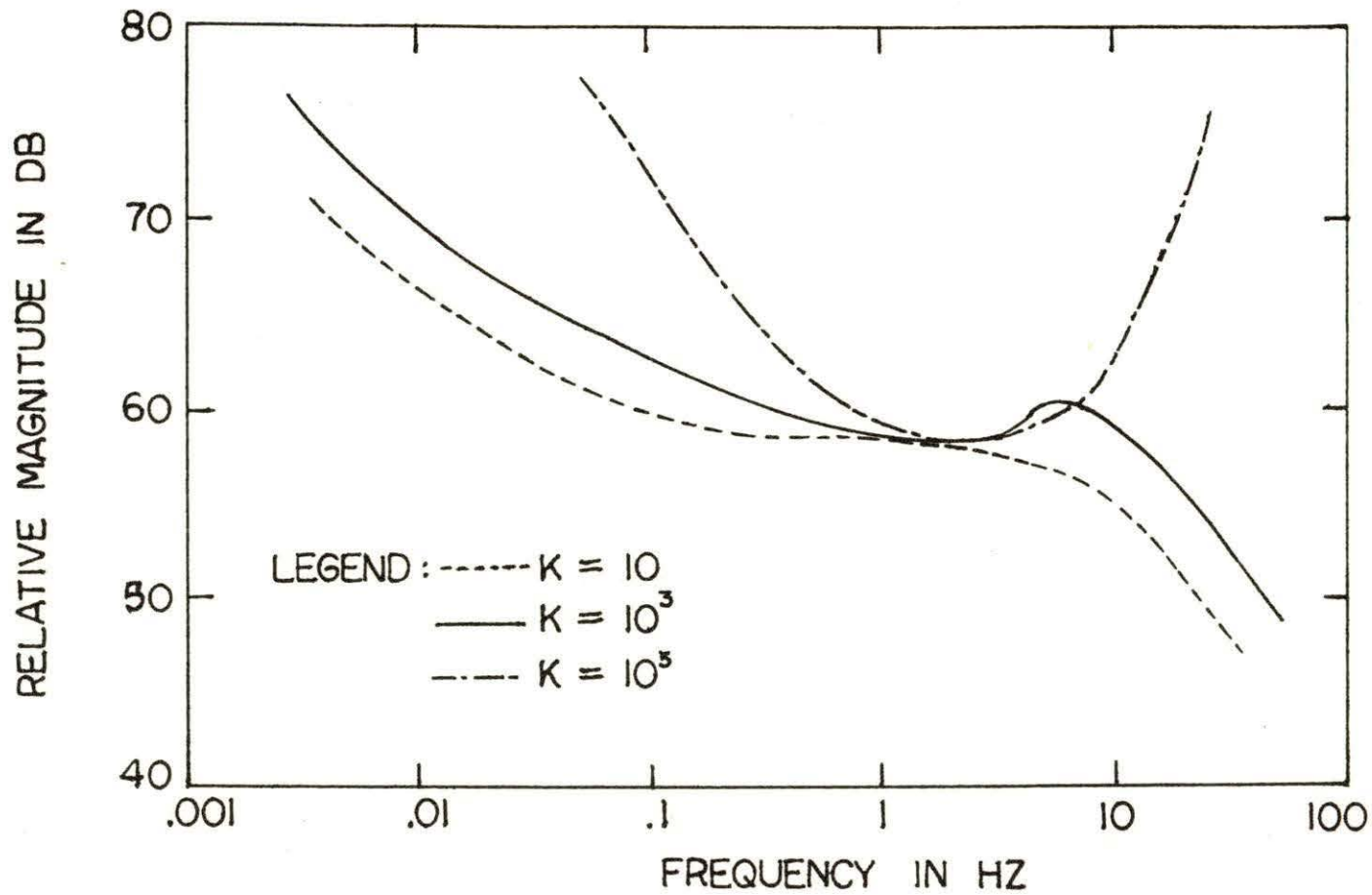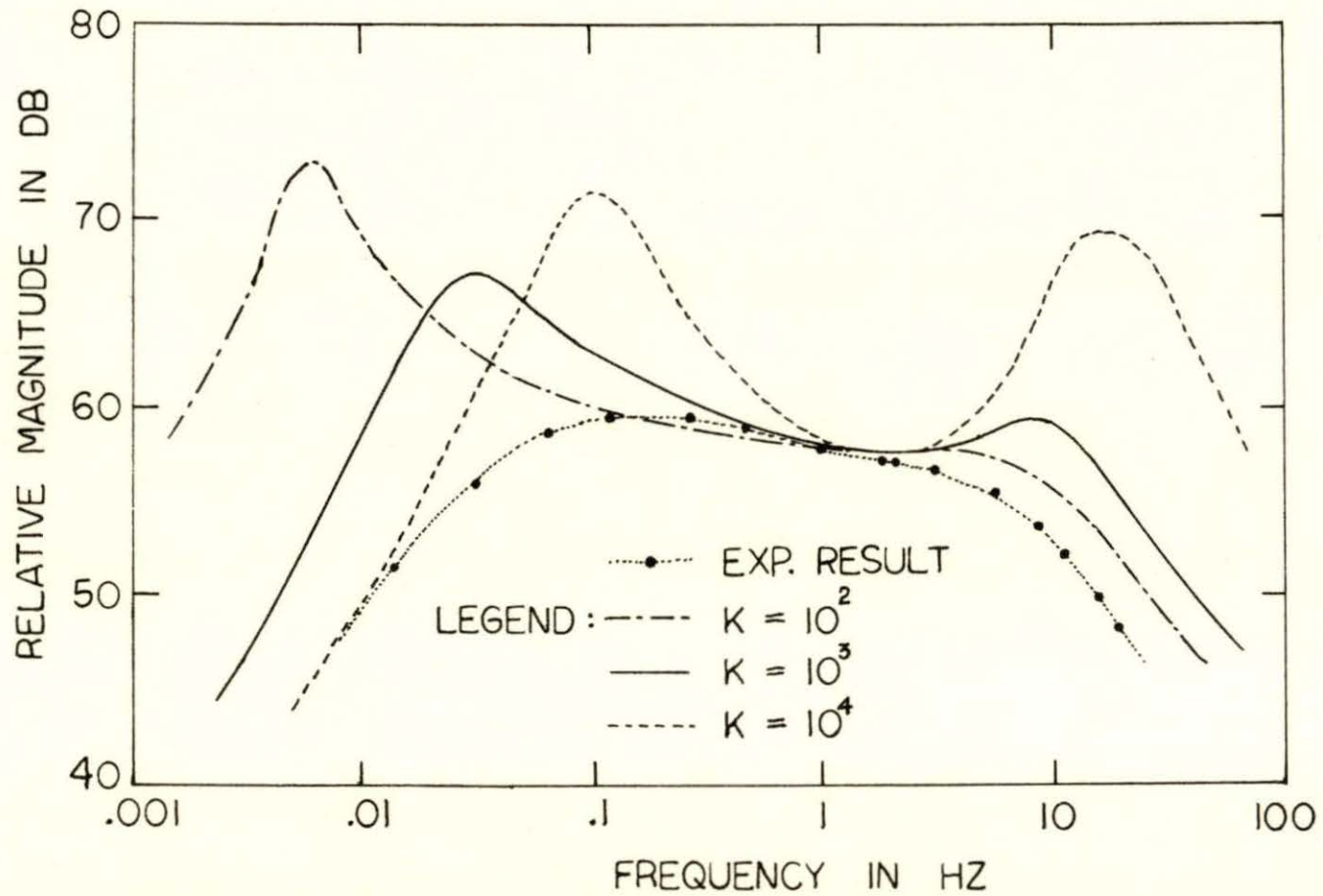
FIGURE 21. MAGNITUDE OF THEORETICAL CLOSED LOOP TRANSFER
FUNCTION WITH I = 100 , T = 2.7 , α P% = 10

FIGURE 22. PHASE ANGLE OF THEORETICAL CLOSED LOOP TRANSFER
FUNCTION WITH $I = 100$, $T = 2.7$, $\alpha P\% = 10$

Figures 19 and 20, are not consistent with the experi-
mental data. When K is equal to 10, the frequency response
has the same characteristic as the open loop. If K
becomes larger, two resonance peaks appear in the magni-
tude and phase angle at both high and low frequencies.

(5) The best theoretical fit to the experimental data, as
shown in Figures 21 and 22, are for K equal 10^3 and $\alpha P\%$,
I, and T equal 10, 100, and 2.7, respectively. At low
frequencies the theoretical phase shift approaches 90
degree and the experimental phase shift is larger than
90 degree. At high frequencies a small resonance peak
is found in the experimental results. Thus, the model
in Figure 3 does not accurately describe the control
loop of the UTR-10.

(6) At high frequencies the experimental frequency response
of the closed loop approaches that of the open loop.

Table V (in Appendix D) shows the normalized standard
deviations of several frequencies in this experiment and re-
veals that σ_G/G (in DB) is less than 0.5% and σ_ϕ/ϕ (in degree)
is less than 2%. Thus, the experimental data of the open
loop (Table III) and closed loop (Table IV) have been shown
to be consistent.

Since there is no relations between the sin-cos func-
tions and the noise signals in the reactor, the cross-correla-
tion of both of them, obtained by repeating several of the

open loop measurement with the oscillator operating outside
the reactor, should be zero. According to Table VI, the
result shows that the capability of the cross-correlation
system for extracting the desired signals from noise signals
is excellent.

From Table III, the differences in the magnitudes in
the forward and reverse rotations at frequencies higher than
2 Hz can be explained if consideration is given to the
presence of higher space modes excited by the oscillator
and the asymmetry of its perturbations in relation to the
core axes.

VI. CONCLUSIONS

Within the scope of this investigation the following conclusions are made.

(1) The techniques of cross-correlation are very useful in extracting information from a noise signal background.

(2) The reactor parameters of the UTR-10 reactor obtained from the experiment are $\beta/\ell = 6.84$ Hz (43.0 rad/sec) and $\overline{\lambda} = 0.058$ Hz (0.367 rad/sec).

(3) For the range of frequencies studies, the kinetics of the coupled-core UTR-10 reactor can be described approximately by a point-reactor model and the frequency response has the same characteristics as that of a single-core reactor as shown by the theory and experiment. However, space dependence was observed in the phase shift at high frequencies.

(4) The open loop transfer function of the UTR-10 reactor shows good agreement with the theoretical transfer function based on the six-group delayed-neutron theory.

(5) The control loop of the UTR-10 reactor with the original console is not well described by the model given by the manufacturer.

VII.   SUGGESTIONS FOR FURTHER WORK

The following suggestions are made for possible future work.

(1)   Use a digital computer system for the cross-correlation technique and data analysis instead of an analog computer.

(2)   Measure experimentally the spatially dependent frequency response of the UTR-10 reactor using different positions of the oscillator and the ion chamber.

(3)   Use the oscillation technique and the rod-drop technique to measure the frequency response of the reactor with different power levels and compare both results.

(4)   Develop a mathematical model to describe the feedback system of the UTR-10 reactor and examine the stability of the system by the experimental methods.

VIII. LITERATURE CITED

1. AMERICAN STANDARD COMPANY, Advanced Technology Laboratories Division, Operating Manual for the UTR-10 Reactor, Mountain View, Calif. (1959).

2. R. AVERY, Proc. Intern. Conf. Peaceful Uses At. Energy, Geneva, 12 182 (1958).

3. J. D. BALCOMB, H. B. DEMUTH and E. P. GYFTOPOULOS, Nucl. Sci. Eng., 11 159 (1961).

4. G. C. BALDWIN, Nucl. Sci. Eng., 6 320 (1959).

5. J. M. BETANCOURT, "Analysis of Coupled Core Reactors Using the Natural Mode Approximation," Ph.D. Dissertation, Iowa State University (1968).

6. C. E. COHN, Trans. Am. Nucl. Soc., 1 162 (1858).

7. H. C. CORBEN, Nucl. Sci. Eng., 6 461 (1959).

8. R. A. DANOFSKY, "Kinetic Behavior of Coupled Reactor Cores," M.S. Thesis, Iowa State University (1960).

9. R. A. DANOFSKY, Personal Communication (April 1971).

10. J. A. DESHONG, JR., "Power Transfer Functions of the EBWR Obtained Using a Sinusoidal Reactivity Driving Function," ANL-5798, Argonne National Laboratory (1958).

11. I. A. ENGEN, "A New Technique for Investigation Feedback and Stability of a Nuclear Reactor," ANL-7686, Argonne National Laboratory (1970).

12. J. P. FRANZ, "Pile Transfer Functions," AECD-3260, Atomic International (1949).

13. C. W. GRIFFIN and J. G. LUNDHOLM, "Measurement of the SRE and KEWB Prompt Neutron Lifetime Using Random Noise and Reactor Oscillator Techniques," NSS-SR-3765, North American Aviation, Inc., Downey, Calif. (1959).

14. G. E. HANSEN, "Kinetics Equation for a Cluster of Rover Reactors," Memorandum N-2-7967, Los Alamos Scientific Laboratory (1965).

15. J. M. HARRER, Nuclear Reactor Control Engineering, pp. 273-316, D. Van Nostrand Co., New York (1963).

16. R. E. HARRER, R. E. BOYAR and D. KRUCOFF, Nucleonics, 8, 10 32 (1952).

17. J. G. LUNDHOLM, C. W. GRIFFIN and E. R. MEISE, "Measurement of Zero Power Frequency Response of the SRE," NAA-SR-3762, North American Aviation, Inc., Downey, Calif. (1959).

18. P. H. LUSTIG, "Transfer Function of UTR-10 Reactor," M.S. Thesis, Iowa State University (1960).

19. M. N. MOORE, Nucl. Sci. Eng., 3 387 (1958).

20. W. C. NODEAN, "The Response of a Coupled Core Reactor to A Localized Oscillation of the Absorption Cross Section," Ph.D. Dissertation, Iowa State University (1969).

21. H. PLAZA and W. H. KOHLER, Nucl. Sci. Eng., 26 419 (1966).

22. V. RAJAGOPAL, Nucl. Sci. Eng., 12 218 (1961).

23. M. W. ROISEN, "Simulation of the UTR-10 Control System on an Analog Computer," M.S. Thesis, Iowa State University (1960).

24. M. A. SCHULTZ, Control of Nuclear Reactors and Power Plants, 2 ed., pp. 85-132, McGraw-Hill, New York (1961).

25. R. L. SEALE, "Coupled-Core Reactors," LAMS-2967, Los Alamos Scientific Laboratory (1964).

26. R. E. SKINNER and D. L. HETRICK, Nucl. Sci. Eng., 3 570 (1958).

27. J. A. THIE, Reactor Noise, Rowman and Littlefield, New York (1963).

28. R. H. UHRIG, Univ. of Florida Symp. Noise Analysis in Nuclear Systems, U. of Fla. (1964).

IX. ACKNOWLEDGMENTS

The author wishes to express his gratitude to his major professor, Dr. Richard Danofsky, Professor of Nuclear Engineering at Iowa State University. His tireless counsel and instructive advice during the investigation are highly appreciated.

A special appreciation is expressed by the author to his father whose financial support made this educational experience possible.

It is also a pleasure to express appreciation to Mr. Thomas Parker for his operation of the reactor during the experiment.

X. APPENDIX A: COUPLED-CORE TRANSFER

FUNCTION DERIVATION

The derivation of the coupled-core transfer function will follow that suggested by Baldwin [4].

It is assumed that the spatial distribution of neutron flux within a slab does not affect the behavior of that region. The reactivity coupling effect is due to the interaction exchange of neutrons between the two regions and it is assumed that the coupling effect of region 2 on region 1 is proportional to the average neutron flux in region 2 and the effect of region 1 on 2 is proportional to the average flux in region 1. The kinetic equations for region 1 are

$$\frac{dn_1(t)}{dt} = \frac{\delta K_1}{\ell_1} n_1(t) - \sum_{i=1}^{6} \frac{dC_{1i}(t)}{dt} + \frac{\alpha_1}{\ell_1} n_2(t-\tau) \tag{43}$$

$$\frac{dC_{1i}(t)}{dt} = \frac{K_1 \beta_i}{\ell_1} n_1(t) - \lambda_i C_{1i}(t) \qquad i = 1,2,\ldots,6 \tag{44}$$

where

$n_1(t)$ = time dependent neutron density in region 1, neutron/cm^3

$C_{1i}(t)$ = time dependent delayed neutron precursor concentration for the i-th group, cm^{-3}

λ_i = i-th group decay constant, sec^{-1}, assumed to be the same in both regions

δK_1 = $K_1 - 1$, reactivity

β_i = delayed neutron fraction of the i-th group with total fraction, assumed to be the same in both regions

ℓ_1 = prompt neutron lifetime, sec

α_1 = coupling coefficient of region 2 on 1

$n_2(t-\tau)$=neutron density in region 2 at some previous time τ, is the delayed time.

Similar equations apply to core two. For simplicity the equations will only be derived for the core one.

Assume an input of the form

$$\alpha_1 = \alpha_1{}^0 + \delta\alpha_1 .$$

The form of the output variables will be

$$n_1 = n_1{}^0 + \delta n_1$$

$$C_{1i} = C_{1i}{}^0 + \delta C_{1i} .$$

Substituting these in the kinetic equations the following is obtained

$$\frac{d}{dt}\,\delta n_1(t) = \frac{\delta K_1}{\ell_1}\,n_1{}^0 + \frac{\delta K_1}{\ell_1}\,\delta n_1(t) - \sum_{i=1}^{6}\frac{d}{dt}\,\delta C_{1i}(t) + \frac{\alpha_1{}^0}{\ell_1}\,n_2{}^0$$

$$+ \frac{\alpha_1{}^0}{\ell_1}\,\delta n_2(t-\tau) + \frac{\delta\alpha_1}{\ell_1}\,n_2{}^0 + \frac{\delta\alpha_1}{\ell_1}\,\delta n_2(t-\tau) \qquad (45)$$

$$\frac{d}{dt}\,\delta C_{1i}(t) = \frac{K_1\beta_i}{\ell_1}\,n_1{}^0 + \frac{K_1\beta_i}{\ell_1}\,\delta n_1(t) - \lambda_i C_{1i}{}^0 - \lambda_i\delta C_{1i}(t). \qquad (46)$$

The second-order term $\frac{\delta\alpha}{\ell_1}\delta n_2(t-\tau)$ may be neglected and from the steady state conditions

$$\frac{\delta K_1}{\ell_1}n_1^0 + \frac{\alpha_1^0}{\ell_1}n_2^0 = 0 \tag{47}$$

$$\frac{K_1\beta_i}{\ell_1}n_1^0 - \lambda_i C_{1i}^0 = 0 \ . \tag{48}$$

Equations (45) and (46) become

$$\frac{d}{dt}\delta n_1(t) = \frac{\delta K_1}{\ell_1}n_1(t) - \sum_{i=1}^{6}\frac{d}{dt}\delta C_{1i}(t) + \frac{\alpha_1^0}{\ell_1}\delta n_2(t-\tau)$$

$$+ \frac{\delta\alpha_1}{\ell_1}n_2^0 \tag{49}$$

$$\frac{d}{dt}\delta C_{1i}(t) = \frac{K_1\beta_i}{\ell_1}\delta n_1(t) - \lambda_i\delta C_{1i}(t) \ . \tag{50}$$

Taking the Laplace transform of the two equations with zero initial condition yields

$$s\Delta N_1(s) = \frac{\delta K_1}{\ell_1}\Delta N_1(s) - \sum_{i=1}^{6}s\Delta C_{1i}(s) + \frac{\alpha_1^0}{\ell_1}\Delta N_2(s)e^{-\tau s}$$

$$+ \frac{n_2^0}{\ell_1}\Delta\alpha_1 \tag{51}$$

$$s\Delta C_{1i}(s) = \frac{K_1\beta_i}{\ell_1}\Delta N_1(s) - \lambda_i\Delta C_{1i}(s) \ . \tag{52}$$

Solve for $C_{1i}(s)$ in Equation (52) and substitute it into Equation (51). Equations (51) and (52) become

$$[\frac{\delta K_1}{\ell_1} - \sum_{i=1}^{6} \frac{K_1\beta_i}{\ell_1} \frac{s}{s+\lambda_i} - s]\Delta N_1(s) + \frac{\alpha_1^0 e^{-\tau s}}{\ell_1} \Delta N_2(s)$$

$$+ \frac{n_2^0}{\ell_1} \Delta\alpha_1(s) = 0. \tag{53}$$

Define $R = n_1^0/n_2^0 =$ the static flux level ratio. From Equation (47), the relation between flux ratio, R, and reactivity, K_1, is

$$\delta K_1 = - \frac{\alpha_1^0}{R}$$

or

$$K_1 = 1 + \delta K_1 = 1 - \frac{\alpha_1^0}{R} .$$

Equation (53) becomes

$$[- \frac{\alpha_1^0}{R\ell_1} - (1 - \frac{\alpha_1^0}{R}) \sum_{i=1}^{6} \frac{\beta_i}{\ell_1} \frac{s}{s+\lambda_i} - s]\Delta N_1(s)$$

$$+ \frac{\alpha_1^0 e^{-\tau s}}{\ell_1} \Delta N_2(s) = - \frac{n_2^0}{\ell_1} \Delta\alpha_1(s) . \tag{54}$$

Multiplying Equation (54) by $- \dfrac{\ell_1 R}{n_1^0 \Delta\alpha_1(s)} = - \dfrac{\ell_1}{n_2^0 \Delta\alpha_1(s)}$

yields

$$[\alpha_1^0 + (R-\alpha_1^0) \sum_{i=1}^{6} \frac{\beta_i s}{s+\lambda_i} + s\ell_1 R] \frac{\Delta N_1(s)}{n_1^0 \Delta\alpha_1(s)}$$

$$- [\alpha_1^0 e^{-\tau s}] \frac{\Delta N_2(s)}{n_2^0 \Delta\alpha_1(s)} = 1 . \tag{55}$$

A similar result for the second core is

$$[\alpha_2{}^0 + (\frac{1}{R} - \alpha_2{}^0) \sum_{i=1}^{6} \frac{\beta_i s}{s+\lambda_i} + s\ell_2 \frac{1}{R}] \frac{\Delta N_2(s)}{n_2{}^0 \Delta\alpha_2(s)}$$

$$- [\alpha_2{}^0 e^{-\tau s}] \frac{\Delta N_1(s)}{n_1{}^0 \Delta\alpha_2(s)} = 1. \tag{56}$$

For simplicity, $\alpha_1 = \alpha_2 = \alpha^0 + \delta\alpha$ is assumed and Equations (55) and (56) become

$$[\alpha^0 + (R-\alpha^0) \sum_{i=1}^{6} \frac{\beta_i s}{s+\lambda_i} + s\ell_1 R] \frac{\Delta N_1(s)}{n_1{}^0 \Delta\alpha(s)}$$

$$- [\alpha^0 e^{-\tau s}] \frac{\Delta N_2(s)}{n_2{}^0 \Delta\alpha(s)} = 1 \tag{57}$$

$$-[\alpha^0 e^{-\tau s}] \frac{\Delta N_1(s)}{n_1{}^0 \Delta\alpha(s)} + [\alpha^0 + (\frac{1}{R} - \alpha^0) \sum_{i=1}^{6} \frac{\beta_i s}{s+\lambda_i}$$

$$+ s\ell_2 \frac{1}{R}] \frac{\Delta N_2(s)}{n_2{}^0 \Delta\alpha(s)} = 1. \tag{58}$$

Consider the one delayed neutron group approximation and simultaneously solve Equations (57) and (58), two transfer functions are obtained as

$$\text{T.F.1} = n_1{}^0 \frac{[\alpha^0 + (\frac{1}{R} - \alpha^0) \frac{\beta s}{s+\bar{\lambda}} + \frac{s\ell_2}{R}] + \alpha^0 e^{-\tau s}}{[\alpha^0 + (R-\alpha^0) \frac{\beta s}{s+\bar{\lambda}} + s\ell_1 R][\alpha^0 + (\frac{1}{R} - \alpha^0) \frac{\beta s}{s+\bar{\lambda}} + s\ell_2 \frac{1}{R}] - \alpha^{0^2} e^{-2\tau s}}$$

$$\tag{59}$$

$$T.F.2 = n_2^0 \frac{[\alpha^0 + (R-\alpha^0)\frac{\beta s}{s+\bar{\lambda}} + s\ell_1 R] + \alpha^0 e^{-\tau s}}{[\alpha^0 + (R-\alpha^0)\frac{\beta s}{s+\bar{\lambda}} + s\ell_1 R][\alpha^0 + (\frac{1}{R}-\alpha^0)\frac{\beta s}{s+\bar{\lambda}} + s\ell_2\frac{1}{R}] - \alpha^{0^2} e^{-2\tau s}} \cdot$$

$$(60)$$

Where β is the total delayed neutron fraction and $\bar{\lambda}$ is the average decay constant.

Assume $R = 1$ and $\ell = \ell_1 = \ell_2$, the coupled-core reactor transfer function reduces to

$$T.F.1 = T.F.2 = \frac{n^0}{\alpha^0(1-e^{-\tau s}) + (1-\alpha^0)\frac{\beta s}{s+\bar{\lambda}} + s\ell} \cdot \quad (61)$$

By a Taylor series expansion, the factor $1-e^{-\tau s}$ may be approximated by τs and Equation (61) becomes

$$T.F. = \frac{n^0}{\ell + \alpha^0\tau} \frac{s+\bar{\lambda}}{s[s+\bar{\lambda} + \frac{(1-\alpha^0)\beta}{\alpha^0\tau + \ell}]}$$

$$= \frac{n^0}{\ell(1 + \frac{\alpha^0\tau}{\ell})} \frac{s+\bar{\lambda}}{s[s+\bar{\lambda} + \frac{(1-\alpha^0)}{1 + \frac{\alpha^0\tau}{\ell}} \frac{\beta}{\ell}]} \cdot$$

Since $\alpha^0 = 0.0155$, $\tau = 2.1 \times 10^{-4}$ sec, $\ell = 1.35 \times 10^{-4}$ sec [8], both terms $\frac{\alpha^0\tau}{\ell}$ and α^0 are very small compared with one and can be neglected.

Equation (62) becomes

$$T.F. = \frac{n^0}{\ell} \frac{s + \overline{\lambda}}{s[s + \overline{\lambda} + \frac{\beta}{\ell}]} \quad .$$

It reveals that the transfer function of the coupled-core reactor is the same as that of the single-core reactor.

XI. APPENDIX B: OPERATION OF THE
LOGIC CIRCUIT

The operation of the logic circuit [9] in Figure 14 is described here. The circuit, including COMP, DIF 1, and AND, is used to count the number of cycles of the sine function (or number of cycles of oscillation) and the circuit, including LP, FFB, FFC, and MT, is used to control the TR-48.

Consider the sine output from the sin-cos potentiometer as applied to the circuit. According to Figure 14, as soon as the sine function drops below zero, $\overline{COMP}$ becomes high. This signal is differentiated by DIF 1 which yields one blip and tries to set FFA. By the time FFA is set (after the next clock pulse) the blip out of DIF 1 has gone by. But if the sine function becomes negative for the next cycle, $\overline{COMP}$ is differentiated as before and the AND gate will yield a blip because FFA is already at the "1" level. From now on this circuit will give a blip each time the sine goes negative. Latching pushbutton (LP) can be used to control the start of a cycle of enabling (E) the flip-flop.

The monostable timer (MT), once activated, runs for a period of time then shuts itself off automatically, the MT output is normally low unless disturbed by a positive going input signal. It is only then that the output becomes high at the next clock pulse, MT remains high for a predetermined

time τ and this τ was adjusted to 10 μsec for this study.

The mode of the TR-48 is controlled by monitoring the OP and RST output from the DES-30 as follows:

OP	RST	TR-48 Mode
0	0	HOLD
0	1	RESET
1	0	OPERATE
1	1	Not Allowed

Consider the MT output as applied to FFB and FFC. After the reset, when FFA is true, MT output goes high, RST becomes low and OP goes high, then the system goes from reset to operate. When the desired number of cycles is reached, the reset (R) of FFC forces the output to the low state while the output of FFB remains low, i.e., OP becomes low and RST remains low. The entire system is then in HOLD. After the value is recorded, the system goes back to the initial state if it is reset. The system is then ready for the next measurement.

XII. APPENDIX C: FORTRAN STATEMENTS

Fortran statement of the open loop transfer function measurement:

```
C       URT-10 OPEN LOOP TRANSFER FUNCTION MEASUREMENTS
  100   FORMAT (9F8.4)
  200   FORMAT (' ',5(F9.4,3X),'FORWARD')
  300   FORMAT (' ',5(F9.4,3X),'REVERSE')
  400   FORMAT (' ',20X,'UTR-10 OPEN LOOP TRANSFER FUNCTION')
  500   FORMAT (' ',30X,'THESIS DATA' //)
  600   FORMAT (' ',4X,'FREQ',7X,'GMAG',9X,'GDB',8X,'PHRAD'
     1          ,6X,'PHDEG',5X,'ROTATION' //)
        WRITE (6,400)
        WRITE (6,500)
        WRITE (6,600)
        J = 0
        M = 198
        G = 0.0
        DB = 0.0
        PRD = 0.0
        PDG = 0.0
        I = 1
   20 READ (5,100) F,T,P0,P1,P2,P4,PAM,X,Y
        IF (I .EQ. 1) GO TO 21
        IF (F .NE. FREQ) GO TO 22
```

```
21 Al = SQRT (X**2 + Y**2)

   CONV = T*P0*P1*P2*P4*PAM

   A2 = Y/X

   A3 = Al/CONV

   G = G + A3

   DB = DB + 20.0*ALOG10(A3)

   PRD = PRD + ATAN(A2)

   PDG = PDG + 57.2957*ATAN(A2)

   FREQ = F

   J = J + 1

   I = I + 1

   IF (I .LE. M) GO TO 20
C     AVERAGE PROCESS
22 Z = FLOAT(J)

   GMAG = G/Z

   GDB = DB/Z

   PHRAD = PRD/Z

   PHDEG = PDG/Z

   IF (A2 .GT. 0.0) GO TO 23

   WRITE (6,200) FREQ,GMAG,GDB,PHRAD,PHDEG

   GO TO 24
23 PHRAD = -(PHRAD)

   PHDEG = -(PHDEG)

   WRITE (6,300) FREQ,GMAG,GDB,PHRAD,PHDEG
24 IF (I .LE. M) GO TO 25
```

```
      STOP
   25 J = 0
      G = 0.0
      DB = 0.0
      PRD = 0.0
      PDG = 0.0
      GO TO 21
      END
```

Fortran statement of the closed loop transfer function

measurement:

```
C      UTR-10 CLOSED LOOP TRANSFER FUNCTION MEASUREMENTS
  100 FORMAT (9F8.4)
  200 FORMAT (' ',5(F9.4,3X),'FORWARD')
  400 FORMAT (' ',20X,'UTR-10 CLOSED LOOP TRANSFER FUNCTION')
  500 FORMAT (' ',30X,'THESIS DATA' //)
  600 FORMAT (' ',4X,'FREQ',7X,'GMAG',9X,'GDB',8X,'PHRAD'
     1         ,6X,'PHDEG',5X,'ROTATION' //)
      WRITE (6,400)
      WRITE (6,500)
      WRITE (6,600)
      J = 0
      M = 43
      G = 0.0
      DB = 0.0
```

```
      PRD = 0.0

      PDG = 0.0

      I = 1

20    READ (5,100) F,T,P0,P1,P2,P4,PAM,X,Y

      IF (I .EQ. 1) GO TO 21

      IF (F .NE. FREQ) GO TO 22

21 A1 = SQRT (X**2 + Y**2)

      CONV = T*P0*P1*P2*P4*PAM

      A3 = A1/CONV

      G = G + A3

      DB = DB + 20.0*ALOG10(A3)

      IF (Y .LT. 0.) GO TO 30

      A2 = ATAN2(Y,X) - 3.1416

      GO TO 31

30 A2 = ATAN2(Y,X) + 3.1416

31 PRD = PRD + A2

      PDG = PDG + 57.2957*A2

      FREQ = F

      J = J + 1

      I = I + 1

      IF (I .LE. M) GO TO 20

22 Z = FLOAT(J)

      GMAG = G/Z

      GDB = DB/Z

      PHRAD = PRD/Z
```

```
PHDEG = PDG/Z

WRITE (6,200) FREQ,GMAG,GDB,PHRAD,PHDEG

IF (I .FT. M) STOP

J = 0

G = 0.0

DB = 0.0

PRD = 0.0

PDG = 0.0

GO TO 21

END
```

XIII. APPENDIX D: TABULATION OF

EXPERIMENTAL DATA

Table III. Experimental result of open loop transfer function

FREQ	GMAG	GDB	PHRAD	PHDEG	ROTATION
17.2000	270.7175	48.6502	-1.5513	-88.8816	FORWARD
14.5000	314.4856	49.9519	-1.4428	-82.6675	FORWARD
13.1400	343.2200	50.7114	-1.3804	-79.0927	FORWARD
11.7000	374.1511	51.4601	-1.3046	-74.7489	FORWARD
10.1600	417.6567	52.4163	-1.2171	-69.7430	FORWARD
9.3500	441.3979	52.8965	-1.1651	-66.7531	FORWARD
7.7000	500.2979	53.9845	-1.0437	-59.7997	FORWARD
5.0200	611.6118	55.7294	-0.7920	-45.3798	FORWARD
2.8000	694.0195	56.8270	-0.5091	-29.1710	FORWARD
3.2950	672.0879	56.5485	-0.7297	-41.8066	FORWARD
2.4600	734.7041	57.3222	-0.6178	-35.3995	FORWARD
1.8400	732.7444	57.2985	-0.5348	-30.6427	FORWARD
1.4800	730.1655	57.2682	-0.4828	-27.6604	FORWARD
1.2550	743.2144	57.4221	-0.4549	-26.0650	FORWARD
1.0750	726.6704	57.2216	-0.4323	-24.7704	FORWARD
0.8670	762.7732	57.6479	-0.4097	-23.4731	FORWARD
0.6540	752.7095	57.5325	-0.3945	-22.6052	FORWARD
0.4230	771.5972	57.7460	-0.3949	-22.6242	FORWARD
0.2500	794.2207	57.9982	-0.4245	-24.3231	FORWARD
0.2040	792.2698	57.9717	-0.4459	-25.5474	FORWARD
0.1650	855.6541	58.6455	-0.4720	-27.0407	FORWARD
0.1550	841.4148	58.4970	-0.4764	-27.2942	FORWARD
0.1180	906.0188	59.1426	-0.5230	-29.9888	FORWARD
0.0745	982.6541	59.8471	-0.6190	-35.4683	FORWARD
0.0584	1059.1550	60.4992	-0.6711	-38.4508	FORWARD
0.0455	1128.6800	61.0514	-0.7152	-40.9759	FORWARD
0.0315	1282.0130	62.1577	-0.7836	-44.8962	FORWARD
0.0220	1465.7550	63.3212	-0.8509	-48.7510	FORWARD
0.0150	1720.8800	64.7148	-0.9205	-52.7424	FORWARD
0.0103	1980.4570	65.9342	-0.9697	-55.5580	FORWARD
0.0086	2085.0070	66.3821	-1.0117	-57.9666	FORWARD
0.0064	2457.2600	67.8090	-1.0678	-61.1799	FORWARD
0.0059	2532.2360	68.0700	-1.0952	-62.7507	FORWARD
20.0000	235.5185	47.4405	-1.5380	-88.1221	REVERSE
17.2000	267.7588	48.5548	-1.4507	-83.1172	REVERSE
14.5500	312.1387	49.8869	-1.3455	-77.0916	REVERSE
13.1500	338.0935	50.5806	-1.2844	-73.5916	REVERSE
11.7000	373.7378	51.4512	-1.2120	-69.4399	REVERSE
10.1700	414.4893	52.3502	-1.1218	-64.2715	REVERSE
9.3600	438.8359	52.8459	-1.0703	-61.3258	REVERSE
7.7200	496.7134	53.9221	-0.9500	-54.4337	REVERSE

Table III (Continued)

FREQ	GMAG	GDB	PHRAD	PHDEG	ROTATION
5.0200	607.8132	55.6754	-0.6938	-39.7529	REVERSE
3.7000	668.2710	56.4990	-0.5377	-30.8064	REVERSE
2.8400	694.0918	56.8282	-0.4234	-24.2580	REVERSE
3.7900	654.9475	56.3240	-0.4097	-23.4744	REVERSE
2.4550	708.0940	57.0018	-0.2284	-13.0866	REVERSE
1.2480	738.0813	57.3621	-0.0697	-3.9913	REVERSE
0.8680	761.5930	57.6344	-0.0269	-1.5416	REVERSE
0.4250	785.6614	57.9046	-0.0124	-0.7116	REVERSE
0.1586	866.7932	58.7583	-0.0837	-4.7940	REVERSE
0.0527	1021.1160	60.1815	-0.2819	-16.1489	REVERSE
0.0306	1253.6160	61.9633	-0.3963	-22.7042	REVERSE
0.0212	2618.7460	67.3655	-0.4597	-26.3387	REVERSE
0.0061	2566.1410	68.1851	-0.7045	-40.3647	REVERSE

Table IV. Experimental result of closed loop transfer function

FREQ	GMAG	GDB	PHRAD	PHDEG	ROTATION
17.2000	270.7175	48.6502	-1.5513	-88.8816	FORWARD
13.1400	343.2200	50.7114	-1.3804	-79.0927	FORWARD
9.3500	441.3979	52.8965	-1.1651	-66.7531	FORWARD
7.7000	500.2979	53.9845	-1.0437	-59.7997	FORWARD
2.8000	684.0195	56.8270	-0.5091	-29.1710	FORWARD
2.4600	734.7041	57.3222	-0.6178	-35.3995	FORWARD
1.8400	732.7444	57.2986	-0.5348	-30.6427	FORWARD
1.6200	724.2720	57.1980	-0.5456	-31.2585	FORWARD
1.5600	731.9973	57.2901	-0.5225	-29.9374	FORWARD
1.0000	778.7673	57.8281	-0.4390	-25.1543	FORWARD
0.4350	870.6841	58.7972	-0.3547	-20.3229	FORWARD
0.2500	914.1970	59.2208	-0.2717	-15.5647	FORWARD
0.1110	923.3726	59.3074	-0.0731	-4.1884	FORWARD
0.0588	855.9482	58.6487	0.2119	12.1410	FORWARD
0.0298	629.2388	55.9760	1.3579	77.8031	FORWARD
0.0124	361.7839	51.1680	2.4878	142.5413	FORWARD

Table V. Normalized standard deviation of the transfer function measurements

FREQ (Hz)	DEVGAN (σ_G/G)	DEVGDB (σ_G/G)	DEVPRD (σ_ϕ/ϕ)	DEVPDG (σ_ϕ/ϕ)
14.5000	0.0030	0.0005	0.0012	0.0012
9.3500	0.0024	0.0004	0.0023	0.0023
2.8000	0.0093	0.0014	0.0099	0.0099
3.2950	0.0011	0.0002	0.0034	0.0034
0.4230	0.0208	0.0032	0.0073	0.0073
0.1550	0.0283	0.0042	0.0170	0.0170
0.0103	0.0161	0.0021	0.0125	0.0125

Where DEVGAN and DEVGDB denote the normalized standard deviations of gain in relative magnitude and decibel, respectively. DEVPRD and DEVPDG denote the normalized standard deviations of phase angle in radian and degree, respectively.

Table VI. Noise rejection capability of the cross-correlation system

FREQ (Hz)	X (output of integrator 30)	Y (output of integrator 31)
20.000	0.0004	0.0010
14.500	0.0005	0.0006
10.160	0.0002	0.0009
7.700	0.0005	0.0002
3.295	-0.0002	-0.0013
2.840	-0.0004	0.0007
1.840	-0.0016	-0.0015
1.255	0.0003	-0.0002
0.869	0.0018	0.0015
0.427	-0.0002	-0.0003